



ARTICLE

SET binding to Sgo1 inhibits Sgo1-cohesin interactions and promotes chromosome segregation

Qianhui Qu^{2*}, Qian Zhang^{1*}, Lu Yang^{1*}, Yujue Chen¹, and Hong Liu¹

At anaphase onset, Sgo1 function of cohesion protection must be disabled to allow timely chromosome segregation, but how this is achieved is not fully understood. Here, we show that SET, a known PP2A inhibitor, directly binds to a domain in Sgo1 in close proximity to the cohesin-binding motif. The Sgo1-cohesin binding can be disrupted by SET in a dose-dependent manner in vitro as well as by SET overexpression in cells, suggesting that SET is also an inhibitor to the Sgo1-cohesin binding. Furthermore, the SET binding-deficient Sgo1 mutant fully supports centromeric cohesion protection but delays chromosome segregation, suggesting that the SET-Sgo1 binding is required for timely chromosome segregation. Moreover, overexpression of SET WT, not the Sgo1 binding-deficient mutant, exacerbates the occurrence of cohesion fatigue in MG132-arrested cells. Conversely, SET depletion delays it. Thus, we propose that a major function of SET during mitosis is to disrupt the Sgo1-cohesin interaction, thereby promoting centromeric cohesion de-protection and timely chromosome segregation at anaphase onset.

Introduction

Timely regulation of centromeric cohesion is essential for proper chromosome segregation and maintaining chromosome stability. Centromeric cohesion is established at S-phase, thereafter maintained until anaphase onset. Its protection at early mitosis requires the conserved complex of the cohesin protector Shugoshin 1 (Sgo1) and phosphatase 2A (PP2A; Kitajima et al., 2006; Riedel et al., 2006; Tang et al., 2006). In human cells, Sgo1 must be localized to the inner centromere (the place between two sister centromeres) to perform its function of cohesion protection (Lee et al., 2008; Liu et al., 2013a, 2015). Efficient installment of Sgo1 to the inner centromere requires Bub1-dependent histone H2A phosphorylation, which promotes Sgo1 binding to nucleosomes, and Cdk1-mediated Sgo1 phosphorylation, which promotes Sgo1 binding to cohesin (Liu et al., 2013a,b). The phosphorylation-enabled Sgo1-cohesin binding is also essential for centromeric cohesion protection. At the metaphase-to-anaphase transition, Sgo1 function of cohesion protection must be disabled to allow timely chromosome segregation (Lee et al., 2008; Liu et al., 2013a). Degradation of Sgo1 by the APC/C at anaphase onset has been suggested to disable Sgo1 function in both mitosis and meiosis (Karamysheva et al., 2009; Jonak et al., 2017). Surprisingly, expression of nondegradable Sgo1 mutants in mitotic cells had little effect on

chromosome segregation (Karamysheva et al., 2009), and a substantial amount of Sgo1 was still retained at early-anaphase kinetochores (Lee et al., 2008), suggesting that Sgo1 degradation might not be the major way to disable its function. At metaphase, tension across sister kinetochores applied by microtubule-pulling force relocates Sgo1 from inner centromeres to kinetochore-proximal regions (hereafter kinetochores; Lee et al., 2008; Liu et al., 2013a), which at the same time separates Sgo1 from centromeric cohesin (Lee et al., 2008). Remarkably, impairment in Sgo1 separation from cohesin has been shown to significantly compromise chromosome segregation (Lee et al., 2008; Liu et al., 2013a), suggesting that removing Sgo1 away from centromeric cohesin may be a critical step toward cohesion resolution. In addition, Sgo2 has also been shown to be separated from centromeric cohesin at metaphase II during meiosis (Lee et al., 2008). All these findings suggest that removing Shugoshin from the inner centromere at metaphase may be a major way to disable its function. However, how this is achieved is not fully understood.

A previous study showed that SET, also termed I2PP2A, plays a critical role in chromosome segregation at anaphase II onset during meiosis (Chambon et al., 2013). SET has been characterized as a cellular PP2A inhibitor (Li et al., 1995, 1996). It was

¹Department of Biochemistry and Molecular Biology and Tulane Aging Center, Tulane University Health Science Center, New Orleans, LA; ²Department of Pharmacology, University of Texas Southwestern Medical Center, Dallas, TX.

*Q. Qu, Q. Zhang, and L. Yang contributed equally to this paper; Correspondence to Hong Liu: hliu22@tulane.edu; Q. Qu's present address is Stanford University, Stanford, CA.

© 2019 Qu et al. This article is distributed under the terms of an Attribution-Noncommercial-Share Alike-No Mirror Sites license for the first six months after the publication date (see <http://www.rupress.org/terms/>). After six months it is available under a Creative Commons License (Attribution-Noncommercial-Share Alike 4.0 International license, as described at <https://creativecommons.org/licenses/by-nc-sa/4.0/>).

thereby proposed that SET may inhibit PP2A activity at anaphase II onset to promote chromosome segregation (Chambon et al., 2013), but compelling evidence to support that SET promotes chromosome segregation through PP2A inhibition is still lacking. SET was also found to interact with Sgo1 by mass spectrometric analysis (Kitajima et al., 2006; Herzog et al., 2012). Not until recently was the biological significance of the Sgo1-SET binding analyzed. In that study, it was demonstrated that SET binding to Sgo1 evicts Sgo1 from chromatin, thus disabling Sgo1 function of cohesion protection (Krishnan et al., 2017). All of these findings spotlight the importance of SET in de-protecting centromeric cohesion at the metaphase-to-anaphase transition. Here we demonstrate that SET can also disrupt the Sgo1-cohesin interaction by directly binding to a domain in Sgo1 that is in close proximity to the cohesin-binding motif. Binding of SET to Sgo1 may be required for timely chromosome segregation. Thus, our findings add a novel dimension in understanding how Sgo1 function is disabled at the metaphase-to-anaphase transition.

Results

SET binds both Sgo1 and Sgo2

In a search for Sgo1-interacting proteins using mass spectrometric analysis, we identified two isoforms of SET (α and β ; Liu et al., 2015). The Sgo1-SET binding has also been reported previously (Kitajima et al., 2006; Herzog et al., 2012). The two SET isoforms differ only in a small portion of amino acid sequences at their N termini and exhibit similar cellular localization and inhibition toward PP2A activity (Saito et al., 1999; Yabe et al., 2014). We therefore speculated that both isoforms may play similar functions and focused on the isoform of SET α (hereafter SET). To confirm the Sgo1-SET binding, Myc-Sgo1 was expressed in nocodazole-arrested HeLa Tet-On cells, and Myc-Sgo1 was immunoprecipitated using antibody against Myc. As shown in Fig. 1 A, both isoforms of endogenous SET and a subunit of a known Sgo1-interacting complex PP2A ($A\alpha$) were pelleted by Myc-Sgo1, confirming SET as one of Sgo1-binding proteins. Moreover, Myc-Sgo1 also interacted with SET in MG132-arrested cells, and no significant difference in Sgo1-SET binding was detected in between nocodazole and MG132 (Fig. S1 A). The Sgo1-SET interaction was further validated by examining the binding between Myc-Sgo1 and GFP-SET simultaneously expressed in HeLa Tet-On cells in both interphase and mitosis (histone H3-pS10; Fig. S1 B). In addition, we identified the endogenous Sgo2-SET interaction by immunoprecipitation (Fig. S1 C). Unfortunately, we failed to detect the endogenous Sgo1-SET binding in nocodazole-arrested cells, suggesting that this binding might be weak or dynamic at early mitosis.

The SET-binding and cohesin-binding domains in Sgo1 are in close proximity, but separable

We then sought to map the regions in Sgo1 that are responsible for SET binding. As the results from a previous *in vitro* cross-linking study identified the N-terminal region (residues 1–72) of Sgo1 interacting with SET (Herzog et al., 2012), we therefore constructed various GST-tagged Sgo1 N-terminal fragments

with distinct lengths and tested their bindings with His₆-tagged SET proteins using GST pull-down assays. We found that GST-Sgo1 fragments with the amino acid sequences of 13–353, 47–353, 115–353, 200–353, and 280–353 robustly bound His₆-SET, but the fragment with the amino acid sequence of 310–353 completely lost its binding to His₆-SET (Fig. 1 B), suggesting that the region 280–310 in Sgo1 is required for the Sgo1-SET binding. Thus, the region 280–310 is the major domain required for SET binding, and we therefore termed this region as SET-binding domain (Fig. 1 C). Notably, the SET-interacting domain in Sgo1 we identified is different from that identified previously (Herzog et al., 2012). The reason behind this discrepancy is unknown but might be due to the application of different assays.

Interestingly, the SET-binding domain (280–310) is in close proximity to the cohesin-binding domain (313–353) that we previously identified (Hara et al., 2014; Fig. 1 C). We then sought to examine whether truncation of the SET-binding domain could affect the binding of Sgo1 to cohesin, and vice versa. To this end, we purified a GST-Sgo1 fragment (241–387) containing both the SET-binding (280–310) and cohesin-binding (313–353) domains in the middle and tested its binding with His₆-SET or a cohesin subcomplex containing SA2 (residues 80–1060) and Scc1 (residues 281–420) using GST pull-down assays. GST-Sgo1 WT was found to bind His₆-SET, and a binding between GST-Sgo1 WT and the cohesin subcomplex was also observed (Fig. 1 D). GST-Sgo1 Δ SET (truncation of the region 280–310 in the fragment 241–387) still interacted with the cohesin subcomplex although it failed to bind SET. Furthermore, GST-Sgo1 Δ cohesin (truncation of the amino acid sequences of 313–353 in the fragment 241–387) still bound SET, while it failed to interact with cohesin. Thus, truncation of either the SET-binding domain or the cohesin-binding domain in Sgo1 barely affects Sgo1 binding to cohesin or SET, respectively, suggesting that these two domains can be separable from each other despite their proximity. This conclusion is further supported by the results from our coimmunoprecipitation experiments on nocodazole-arrested HeLa Tet-On cells. In these experiments, we also evaluated the extent to which the N-terminus (residues 1–40) of Sgo1 contributes to the Sgo1-SET binding. As shown in Fig. 1 E, Myc-Sgo1 WT robustly bound GFP-SET, whereas Myc-Sgo1 Δ SET and Δ SET Δ N completely lost their binding to GFP-SET. Furthermore, Myc-Sgo1 Δ N still maintained binding to GFP-SET as Myc-Sgo1 WT did (Fig. 1 F). These results suggest that the SET-binding domain (280–310) in Sgo1 is the major binding site for SET, and the N-terminus (residues 1–40) of Sgo1 is dispensable for SET binding in cells. In addition, we also found that Myc-Sgo1 WT, Δ SET, Δ N, and Δ SET Δ N all bound Smc1, a cohesin subunit, and PP2A at comparable levels (Fig. 1 G). Taking all the results together, we concluded that the cohesin-binding and SET-binding domains in Sgo1 are separable.

Sgo1 Δ SET mutants localize at centromeres and fully support centromeric cohesion

We next examined the cellular localization of Sgo1 Δ SET mutants. At early mitosis, Sgo1 is recruited through its C-terminal basic domain to the kinetochore by directly binding to Bub1-mediated H2A phospho-Thr120 (Kawashima et al., 2010; Liu

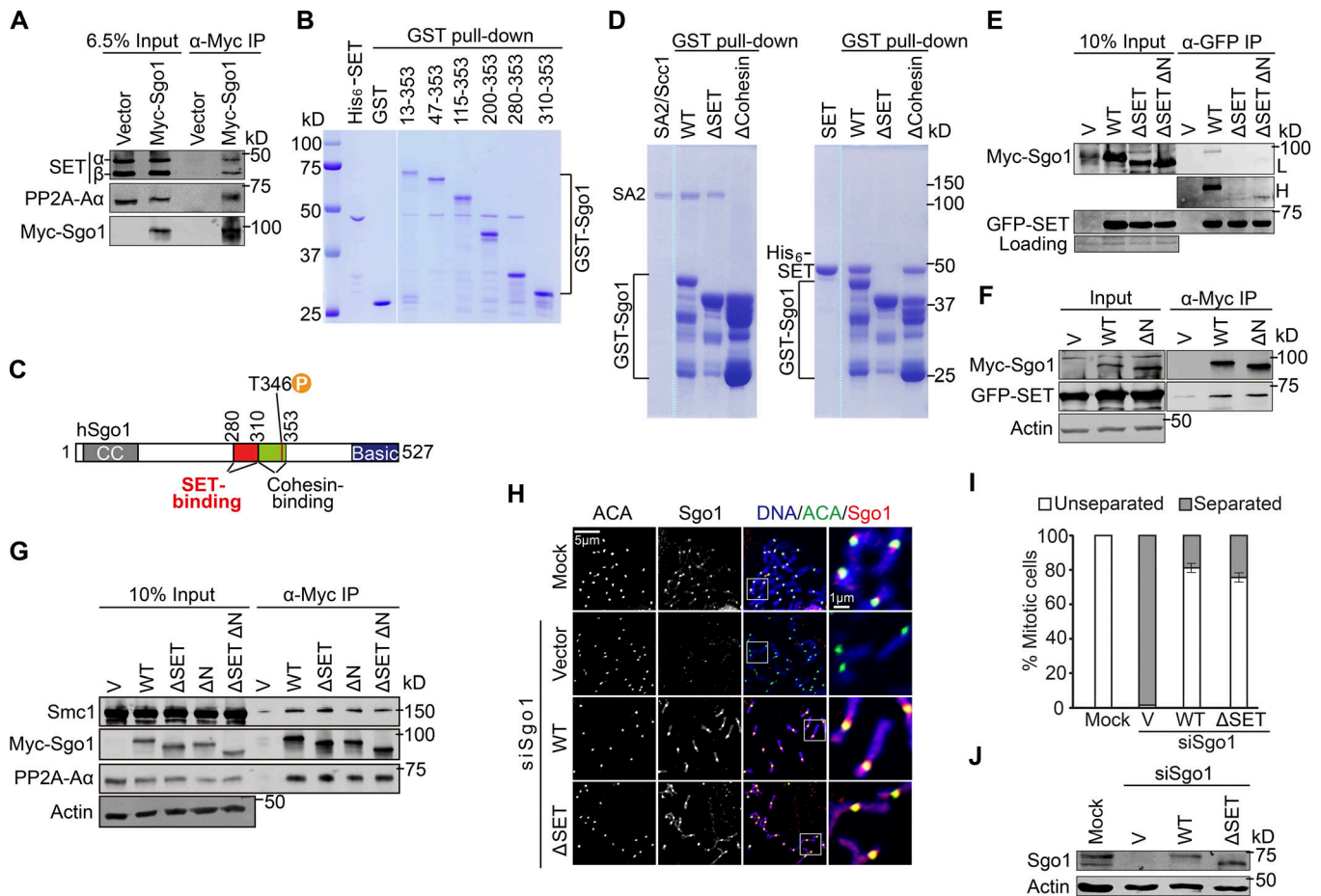


Figure 1. SET binds to a domain in Sgo1 that is close proximity to the cohesin-binding domain, and Sgo1 Δ SET mutants fully support centromeric cohesion. (A) Myc-Sgo1 binds both isoforms of endogenous SET. Lysates of nocodazole-arrested HeLa Tet-On cells stably expressing Myc-Sgo1 were incubated with antibody against Myc. Pelleted proteins were resolved on SDS-PAGE and blotted with the indicated antibodies. IP, immunoprecipitation. (B) Mapping the domains in Sgo1 interacting with SET. GST proteins and GST-tagged Sgo1 fragments with the indicated lengths were incubated with His₆-SET (full length) proteins, and GST pull-down assays were performed. The pelleted proteins were resolved on SDS-PAGE and stained with Coomassie blue. (C) Schematic drawing of the functional domains in human Sgo1. (D) Recombinant GST-Sgo1 fragments were incubated with a cohesin sub-complex containing SA2 and Scc1 (left panel), or His₆-SET full length (right panel). The GST bead-bound proteins were resolved with SDS-PAGE and stained with Coomassie blue. SA2: 80–1060; Scc1: 281–420; GST-Sgo1 WT: 241–387; Δ SET: 241–387 depleted of 281–310; and Δ Cohesin: 241–387 depleted of 313–353. Notably, Scc1 fragments are invisible in the gel stained with Coomassie blue, likely due to small size and small amount. Therefore, it was not labeled. The gels were spliced from the same ones. (E) The SET-binding domain in Sgo1 is required for the Sgo1–SET binding in cells. Lysates of mitotic HeLa Tet-On cells transfected with vectors (V) or plasmids containing GFP-SET and Myc-Sgo1 WT or Δ SET or Δ SET Δ N were incubated with antibody against GFP. The immunoprecipitated proteins were resolved with SDS-PAGE and blotted with the indicated antibodies. WT, Sgo1 full length; Δ SET, Sgo1 truncated of the region 281–310; Δ SET Δ N, Sgo1 truncated of the regions 1–40 and 281–310. The loading control is defined with a nonspecific Western blot band that appears in each lane. (F) The N-terminus (1–40) of Sgo1 is dispensable for the Sgo1–SET binding in cells. Lysates of nocodazole-arrested HeLa Tet-On cells transfected with vectors (V), plasmids containing GFP-SET and Myc-Sgo1 WT or Δ N were incubated with antibody against Myc. The immunoprecipitated samples were resolved with SDS-PAGE and blotted with the indicated antibodies. (G) The SET-binding domain and the N-terminus (1–40) in Sgo1 are dispensable for the Sgo1–cohesin binding in cells. Lysates of nocodazole-arrested HeLa Tet-On cells transfected with vectors (V) or plasmids containing Myc-Sgo1 WT, Δ SET, Δ N, or Δ N Δ SET were incubated with antibody against Myc. The immunoprecipitated proteins were resolved with SDS-PAGE and blotted with the indicated antibodies. (H) RPE-1 cells stably expressing exogenous Sgo1 WT or Δ SET were treated with Sgo1 siRNAs. Representative images of chromosome spread from nocodazole (3 h)-arrested RPE-1 cells are shown here. The outlined regions are amplified and shown in the right panel. (I) Quantification of cells with unseparated and separated sister chromatids in H. Unseparated sister chromatids were defined as the chromosome morphology described in Mock (H), and separated sister chromatids were defined as the chromosome morphology described in siSgo1 (H). Averages and standard deviations from two independent experiments are shown here. More than 30 cells for each condition were examined. (J) Cell lysates in H were separated with SDS-PAGE and blotted with the indicated antibodies.

et al., 2015). The inner-centromeric localization of Sgo1 is mediated by Cdk1 phosphorylation-enabled Sgo1–cohesin interaction, which is essential for centromeric cohesion protection as well (Liu et al., 2013a,b). Because the Sgo1 Δ SET mutant retains the cohesin-binding domain and C-terminal basic domain, we

reasoned that this mutant could localize normally at inner centromeres as WT does. To test this, we constructed the RPE-1 cells stably expressing Sgo1 WT or Δ SET and then examined their cellular localization. The results from Western blots showed that the exogenous Sgo1 WT and Δ SET proteins were

expressed at similar levels to the endogenous Sgo1 proteins (Fig. 1 J). As shown in Fig. 1 H, Sgo1 localized at centromeres in mock cells, and siSgo1 treatment largely abolished the Sgo1 signals at centromeres. As expected, expression of exogenous Sgo1 WT or Δ SET restored their centromeric localization, though we noticed that the intensities of both exogenous Sgo1 WT and Δ SET were stronger than the one of endogenous Sgo1 in mock cells. The similar localization patterns were also observed in HeLa Tet-On cells expressing Myc-Sgo1 WT, Δ SET, or Δ N (Fig. S1 D). Thus, the SET-binding domain in Sgo1 is dispensable for its centromeric localization during mitosis.

Consistent with the previous findings, Sgo1 depletion induced massive centromeric cohesion defects in 99% RPE-1 cells (Tang et al., 2006; Fig. 1 I). Expression of the exogenous Sgo1 WT or Δ SET significantly rescued the cohesion defects and restored the centromeric cohesion in 81% or 75% of RPE-1 cells, respectively (Fig. 1 I). In the remaining \sim 20% cells in which centromeric cohesion was not restored, the centromeric Sgo1 signals were barely detectable. Taken all together, we concluded that the SET-binding domain in Sgo1 is not important for its function of cohesion protection at early mitosis.

Identification of the domains in SET responsible for Sgo1 binding

We next sought to identify the residue(s) in SET that are responsible for Sgo1 binding. A previous cross-linking study demonstrated that the N-terminal region (1–200), not the C-terminal region (201–290), of SET interacts with Sgo1 (Herzog et al., 2012). The structure study showed that the region 25–78 in SET- β , corresponding to the region 38–91 in SET- α , adopts a helix structure to mediate SET dimerization (Muto et al., 2007). It is conceivable that this region might also be involved in Sgo1 binding. To identify the residues responsible for Sgo1 binding, we mutated many of the residues in this region that are not involved in SET dimerization and tested their binding with Sgo1 (Muto et al., 2007). We also examined the residues that were found to cross-link with Sgo1 in the cross-link study (Herzog et al., 2012). In vitro translated S35-radiolabeled SET WT or mutant proteins were mixed with recombinant GST-Sgo1 fragments with the amino acid sequence of 241–350 containing the SET-binding domain (280–310), and GST pull-down assays were performed. We found that single mutations of D56K, E60K, and E64K significantly diminished the Sgo1-SET binding (Fig. 2 A and Fig. S2 A). Single mutations of E40K, E46K, E50K, K68E, and K72E were also found to decrease the Sgo1-SET binding, but the extents were milder than the former three mutations. Thus, our results indicate that the N-terminal coil domain of SET interacts with Sgo1, which is consistent with the previous cross-linking data (Herzog et al., 2012). Because our subsequent results demonstrated that the SET 3K (triple mutations of D56K, E60K, and E64K) mutant almost completely loses its binding to Sgo1 in cells, we mainly concentrated on these three sites, not on the others. As SET has been shown to bind histone proteins (Matsumoto et al., 1999), we also tested the binding between histone and these SET mutants. Interestingly, none of these mutations significantly affected their binding to bulk histone proteins (Fig. S2 B). We next constructed SET 3K mutants

(D56K/E60K/E64K), hoping to more efficiently disrupt the Sgo1-SET binding, and then tested the binding between SET 3K and Sgo1 using in vitro binding assays. As shown in Fig. 2 B, GST-SET WT efficiently pelleted S35-radiolabeled Sgo1, but GST-SET 3K failed to do so. A similar result was also observed between SET and S35-radiolabeled Sgo2 (Fig. 2 C). Thus, SET is a Shugoshin-binding protein, and it binds to Sgo1 through a region near its N-terminus (residues 38–72; Fig. 2 A). We then sought to verify whether triple mutations of D56K, E60K, and E64K were able to disrupt the Sgo1-SET binding in cells as well. Both Myc-Sgo1 (1–472) and GFP-SET were expressed in HeLa Tet-On cells followed by GFP antibody-mediated immunoprecipitation. Consistent with the in vitro binding result in Fig. 2 B, GFP-SET WT robustly bound Myc-Sgo1, but 3K poorly did so (Fig. 2 D), suggesting that triple mutations of D56K E60K, and E64K are sufficient to largely disrupt the Sgo1-SET interaction in cells.

SET has also been found to interact with PP2A and nucleosomes and form homodimers with itself (Li et al., 1995, 1996; Matsumoto et al., 1999; Muto et al., 2007). We then tested if the SET 3K mutant exhibited any defects in binding to these partners. GFP-SET WT, 3K, or Δ C was expressed in HeLa Tet-On cells, and immunoprecipitation was performed using antibody against GFP. GFP-SET 3K pelleted PP2A-A α as efficiently as WT did, whereas GFP-SET Δ C (residues 1–226) failed to do so under the same conditions (Fig. 2 E). We also observed that GFP-SET 3K made interactions with histone H3 comparable to WT (Fig. 2 F). As the triple mutations fall within the region that is responsible for SET dimerization, we thereby tested whether these mutations could impair SET dimerization as well. To achieve it, we tagged SET with Myc and GFP, respectively, and then tested the binding between them. Myc-SET WT or 3K and GFP-SET WT or 3K were simultaneously expressed in HeLa Tet-On cells, and immunoprecipitation was performed using antibody against Myc. We found that Myc-SET bound with GFP-SET for both WT and 3K at a comparable level (Fig. 2 G). Thus, the SET 3K mutant only exhibits binding defects to Sgo1 among all the tested binding partners. It is a separation-of-function mutant. We further tested if SET Δ C is also a separation-of-function mutant. Surprisingly, this mutant not only lost its binding to PP2A (Fig. 2 E), but also exhibited reduced binding to Sgo1 (Fig. S2 C). We thereby mainly used the SET 3K mutant in the subsequent experiments.

SET can disrupt the Sgo1-cohesin interaction in vitro and in cells

Because the SET- and cohesin-binding domains in Sgo1 are in close proximity, we speculated that SET and cohesin could compete with one another for binding Sgo1. To test this, we performed in vitro competition assay using recombinant proteins. His₆-SET (full length) proteins were added into the mixture of GST-Sgo1 (Cdk1-phosphorylated: phospho-Sgo1 or nonphospho-Sgo1) proteins and the cohesin subcomplex containing SA2 (residues 80–1060) and Scc1 (residues 281–420) in a dose-dependent manner. GST-Sgo1 proteins were pelleted by GST beads. As we have previously shown that Cdk1 phosphorylation of Sgo1 at Thr346 significantly enhances the Sgo1-cohesin binding (Liu et al., 2013b; Hara et al., 2014), inclusion of

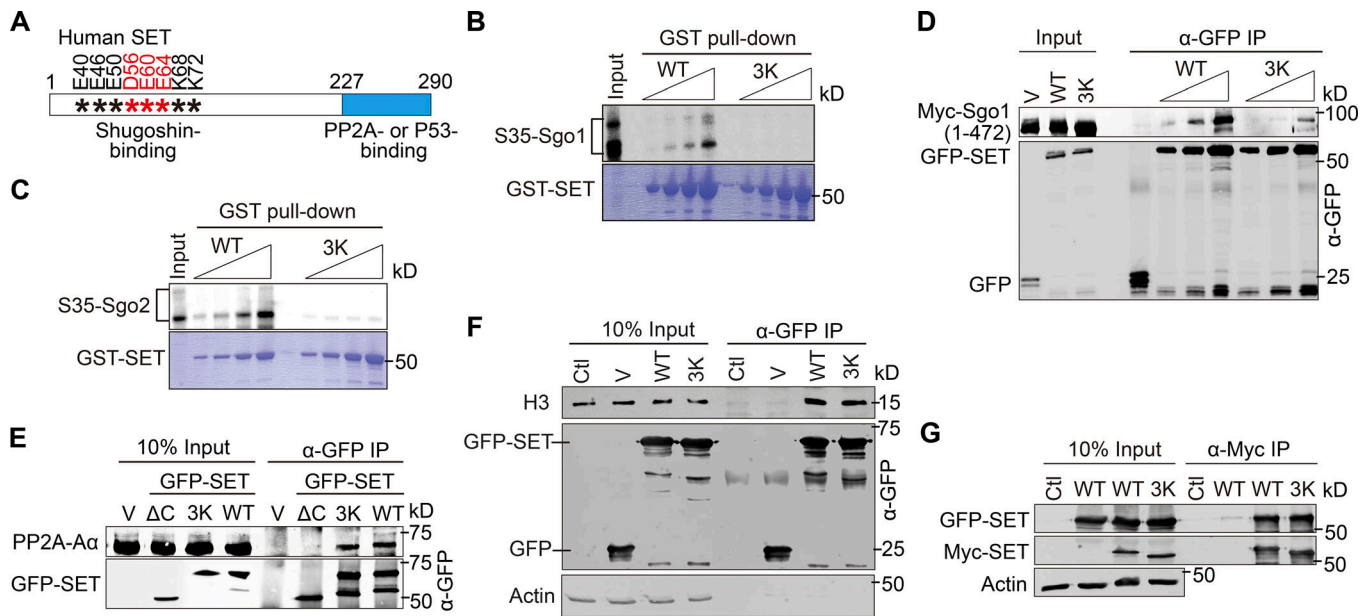


Figure 2. Identification of the domains in SET responsible for binding Sgo1. (A) Schematic drawing of the functional domains of human SET. The residues that are important for the Sgo1–SET interaction were labeled, and the red ones were chosen for the subsequent studies. (B and C) Triple mutations (3K) of D56K, E60K, and E64K abolish Shugoshin–SET interactions in vitro. In vitro–translated S35–radiolabeled human Sgo1 (B) and human Sgo2 (C) were incubated with recombinant GST–SET (full length) WT or 3K proteins. GST bead–pelleted proteins were resolved with SDS–PAGE and stained with Coomassie blue. Dried gels were visualized by a phospho–imager. (D) Triple mutations (3K) of D56K, E60K, and E64K abolish the Sgo1–SET interaction in cells. Lysates of mitotic HeLa Tet–On cells transfected with vectors (V) or plasmids containing Myc–Sgo1 (1–472) and GFP–SET WT or 3K (D56K/E60K/E64K in SET– α) were incubated with antibody against GFP. The immunoprecipitated proteins with distinct doses were resolved with SDS–PAGE and blotted with the indicated antibodies. (E and F) Triple mutations (3K) of D56K, E60K, and E64K barely affect SET binding to PP2A and histones. Lysates of nocodazole–arrested HeLa Tet–On cells transfected with vectors (V) or plasmids containing GFP–SET WT, 3K, or SET Δ (truncation of the region 227–290 in SET– α ; E) were treated with anti–GFP antibody. The immunoprecipitated proteins were resolved with SDS–PAGE and blotted with the indicated antibodies. Control (Ctl) in F denotes mock transfection without vectors. (G) Triple mutations (3K) of D56K, E60K, and E64K do not affect SET dimerization. Lysates of nocodazole–arrested HeLa Tet–On cells transfected with vectors (Ctl) or plasmids containing GFP–SET (WT or 3K) and Myc–SET (WT or 3K) were incubated with antibody against Myc. The pelleted proteins were resolved with SDS–PAGE and blotted with the indicated antibodies.

phospho–Sgo1 in this experiment would enable us to evaluate in more detail how SET competes with cohesin for Sgo1 binding. As shown in Fig. 3 A, SET disrupted the Sgo1–cohesin binding in a dose–dependent manner regardless of the phosphorylation state of Sgo1 at T346. We failed to observe a significant difference in resisting SET competition between mock–treated and Cdk1–treated Sgo1. Because we could not quantitatively measure how much Sgo1 was phosphorylated by Cdk1 in this in vitro experiment, the above result might be due to an outcome of low efficiency in Cdk1 phosphorylation. Thus, SET can function as an inhibitor to the Sgo1–cohesin interaction in vitro.

To verify that SET can also inhibit the Sgo1–cohesin interaction in cells, we examined the amount of endogenous Sgo1–immunoprecipitated cohesin in HeLa Tet–On cells with or without GFP–SET overexpression. Congruent with the in vitro result, GFP–SET overexpression moderately reduced the Sgo1–cohesin binding by more than twofold (Fig. 3, B and C). To further confirm if the disruption of the Sgo1–cohesin interaction is mediated by SET binding to Sgo1, we compared the amount of Smc1 immunoprecipitated by Myc–Sgo1 in HeLa Tet–On cells overexpressing GFP–SET WT and 3K. Consistently, Myc–Sgo1 bound more GFP–SET but less Smc1 in cells expressing GFP–SET WT than vector control; in contrast, expression of GFP–SET

3K barely affected the Myc–Sgo1–Smc1 binding but decreased its binding with Myc–Sgo1 (Fig. 3, D and E). Furthermore, we expressed GFP–SET at distinct levels and found that SET disrupted the Sgo1–cohesin interaction in a dose–dependent manner (Fig. 3 F). Altogether, these observations suggest that SET binding to Sgo1 can, at least moderately, inhibit the Sgo1–cohesin interaction in cells. As Cdk1–phosphorylated Sgo1 at Thr346 is essential for the Sgo1–cohesin interaction (Liu et al., 2013b), we examined Sgo1 phospho–Thr346 levels in cells overexpressing SET. We found that Sgo1 phospho–Thr346 levels were comparable in mock cells and cells expressing GFP–SET WT or 3K (Fig. 3, D and G), suggesting that the difference in the Sgo1–cohesin binding observed above is unlikely due to changes in phospho–Thr346 levels. In addition, no significant difference was detected in Sgo1–PP2A interactions in GFP–SET WT and 3K cells (Fig. 3 D).

Chromosome segregation is delayed in cells expressing Sgo1 Δ SET or depleted of SET

The Peters laboratory has systematically analyzed chromosome segregation in response to delayed cohesion resolution induced by Separase depletion or expression of noncleavable cohesin subunits (Hauf et al., 2001; Waizenegger et al., 2002). They found that Separase depletion or expression of noncleavable

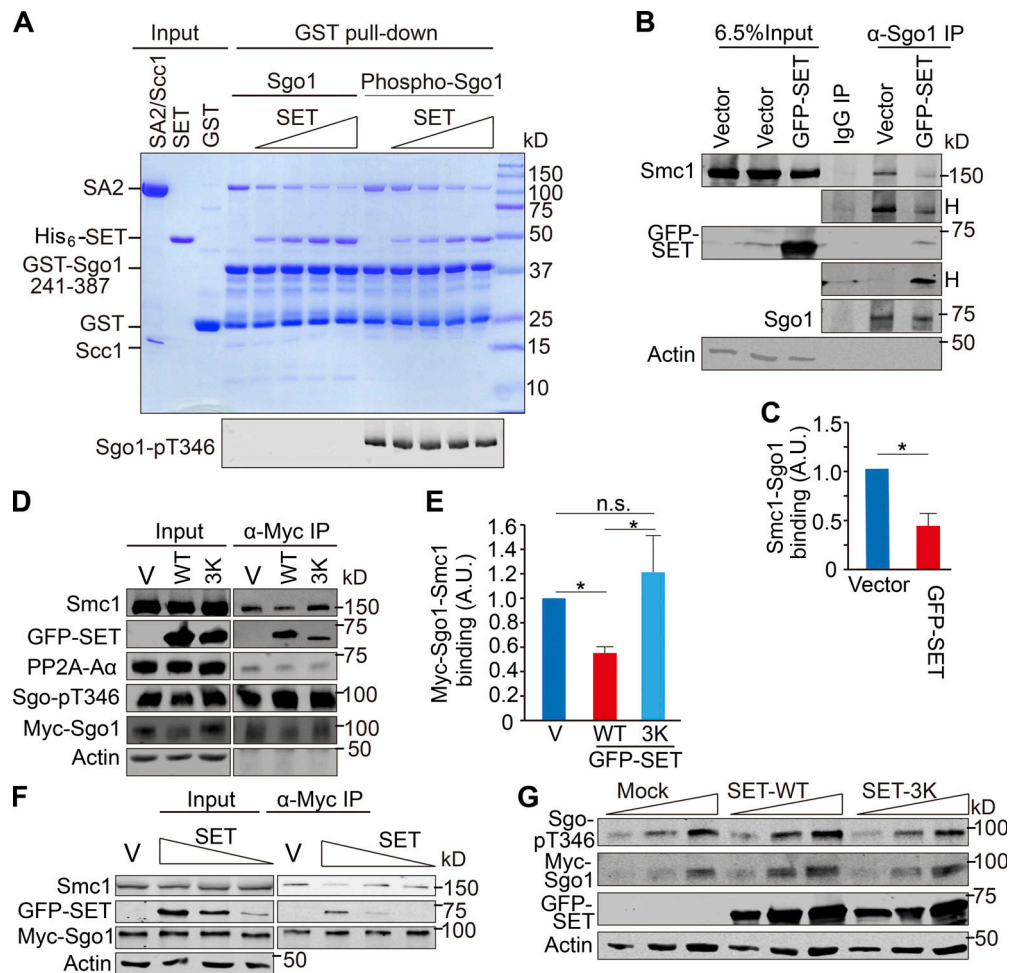


Figure 3. SET binding to Sgo1 inhibits the Sgo1-cohesin interaction in cells and in vitro. (A) SET binding to Sgo1 inhibits the Sgo1-cohesin interaction in vitro. Recombinant SA2/Sccl1 complexes (SA2: 80–1060; Sccl1: 281–420) were incubated with GST-Sgo1 fragments (241–387) in the presence or absence of Cdk1/cyclin B1. GST pull-down was performed in the presence of His₆-SET with increasing concentrations. Pelleted proteins were resolved with SDS-PAGE, stained with Coomassie blue, or blotted with antibody against Sgo1 pT346. (B) SET overexpression weakens the endogenous Sgo1-cohesin interaction. Lysates of nocodazole-arrested HeLa Tet-On cells transfected with vectors or plasmids containing GFP-SET were incubated with IgG or with antibody against Sgo1. The immunoprecipitated proteins were resolved with SDS-PAGE and blotted with the indicated antibodies. H denotes heavier exposure. (C) Quantification of Sgo1-bound Smc1 in B. A two-tailed t-test was performed for the experiments. Quantification details were recorded in the section of Antibodies, immunoblotting, and immunoprecipitation in Materials and methods. Averages and standard deviations were calculated based on two independent experiments. *, P < 0.05. (D) Overexpression of SET WT, not 3K, moderately weakens the Myc-Sgo1-cohesin interaction in cells. Lysates of nocodazole-arrested HeLa Tet-On cells stably expressing Myc-Sgo1 (1–472) transfected with vector controls (V) or plasmids containing GFP-SET WT or 3K were incubated with antibody against Myc. The immunoprecipitated proteins were resolved with SDS-PAGE and blotted with the indicated antibodies. (E) Quantification of Myc-Sgo1-bound Smc1 in D. One-way ANOVA was performed followed by pairwise comparisons using Tukey's test. Quantification details were recorded in the section of Antibodies, immunoblotting, and immunoprecipitation in Materials and methods. Means and standard deviations were calculated based on three independent experiments. *, P < 0.05. n.s., not significant. (F) SET disrupts the Sgo1-cohesin binding in a dose-dependent manner. Lysates of nocodazole-arrested HeLa Tet-On cells stably expressing Myc-Sgo1 (1–472) transfected with vectors or different doses of plasmids containing GFP-SET were incubated with antibody against Myc-Sgo1. The immunoprecipitated proteins were resolved with SDS-PAGE and blotted with the indicated antibodies. (G) SET overexpression does not affect Sgo1 pT346 levels. Nocodazole-arrested HeLa Tet-On cells stably expressing Myc-Sgo1 (1–472) were transfected with vectors (Mock) or plasmids containing GFP-SET WT or 3K. Different doses of cell lysates were loaded, resolved on SDS-PAGE, and blotted with the indicated antibodies.

cohesin subunits significantly delayed chromosome segregation at metaphase-to-anaphase transition, suggesting that delayed cohesion resolution can postpone chromosome segregation. As SET plays an important role in cohesion regulation, we also monitored chromosome segregation in SET-depleted RPE-1 cells expressing H2B-GFP using time-lapse analysis. Mock cells spent an average of 17 min in establishing metaphase plates from nuclear envelope breakdown (NEB), and another 14 min in initiating chromosome segregation (Fig. 4, A and B; and Fig. S3 A).

Separase depletion did not significantly affect the average duration (17.1 min) from NEB to metaphase, either, but instead significantly delayed the duration of metaphase to chromosome segregation, with an average of 30 min, which is consistent with the findings from the Peters group. Interestingly, similar to Separase depletion, SET depletion did not alter the average duration from NEB to metaphase, either (17.5 min), but instead significantly delayed chromosome segregation, with an average duration of 23.1 min. Thus, SET functions to promote timely

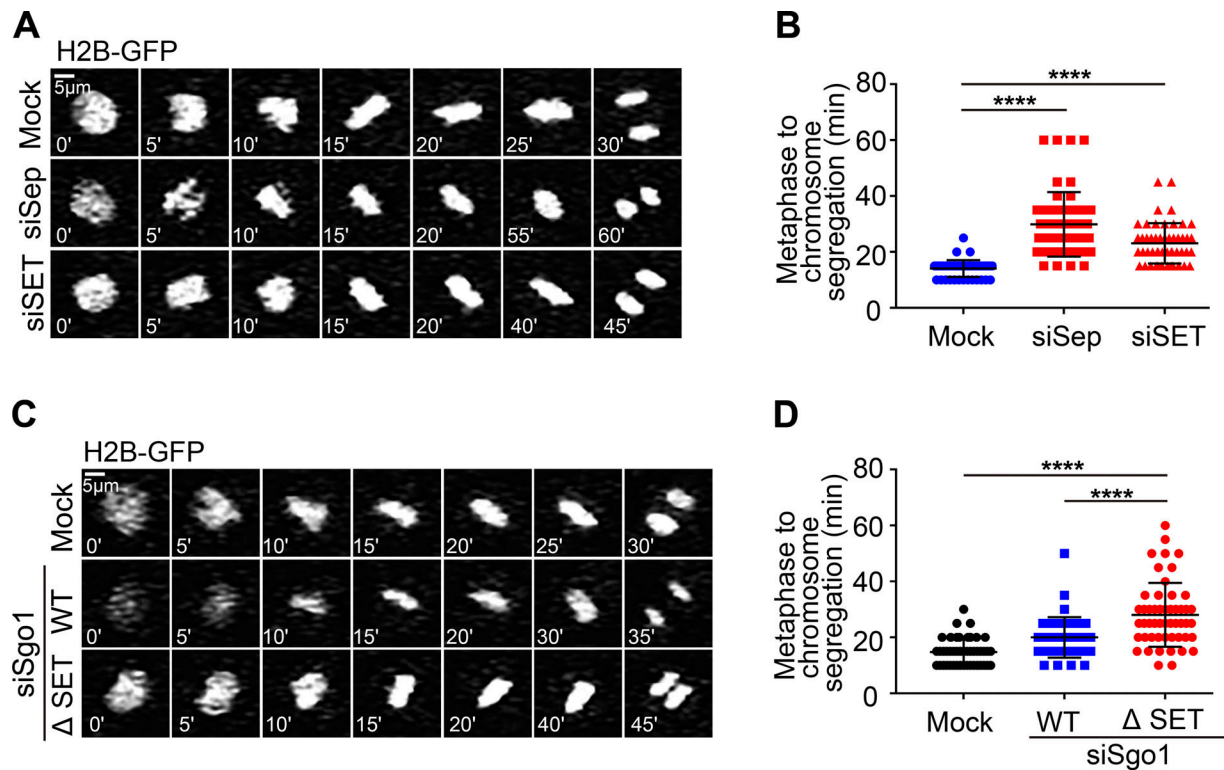


Figure 4. Expression of Sgo1 Δ SET or SET depletion delays chromosome segregation. (A) Time-lapse analysis of RPE-1 cells expressing H2B-GFP and transfected with Mock, Separate (Sep), or SET siRNAs. (B) Quantification of the duration from metaphase to chromosome segregation of mitotic cells in A. The average and standard deviation are shown here. Mock, $n = 50$ cells; siSep, $n = 50$ cells; siSET, $n = 50$ cells. ****, $P < 0.0001$. One-way ANOVA was performed followed by pairwise comparisons using Tukey's test. (C) Time-lapse analysis of H2B-GFP RPE-1 cells stably expressing exogenous Sgo1 WT or Δ SET transfected with luciferase (Mock) or Sgo1 siRNAs. (D) Quantification of the duration from metaphase to chromosome segregation in mitotic cells in C. The average and standard deviation are shown here. Mock, $n = 45$ cells; WT, $n = 41$ cells; Δ SET, $n = 51$ cells. ****, $P < 0.0001$. One-way ANOVA was performed followed by pairwise comparisons using Tukey's test.

chromosome segregation during mitosis, which is consistent with the previous findings (Krishnan et al., 2017).

To further explore the importance of the SET-Sgo1 binding in chromosome segregation, we examined mitotic progression in Sgo1 Δ SET cells. RPE-1 cells stably expressing Sgo1 WT or Δ SET were transfected with plasmids containing GFP-H2B and Sgo1 siRNAs. Time-lapse analysis was performed to monitor chromosome behavior during mitosis. Mock cells progressed from NEB to metaphase with an average duration of 16.3 min, and Sgo1 depletion arrested the cells in prometaphase with an average duration of 200 min (Fig. 4, C and D; and Fig. S3 B). These arrested cells finally underwent cell death or abnormally exited from mitosis. Expression of Sgo1 WT or Δ SET significantly rescued the prometaphase arrest caused by Sgo1 depletion in ~80% of cells. In the remaining 20% of cells, no obvious rescue was observed. As low or no expression of Sgo1 WT or Δ SET was observed in ~20% cells (Fig. 1 I), we reasoned that the inefficient Sgo1 expression could be the cause of failure in rescuing the prometaphase arrest. Therefore, we only quantified the cells in which the duration from NEB to metaphase has largely been rescued. The cells expressing with Sgo1 WT or Δ SET progressed from NEB to metaphase with average durations of 17 min or 17.1 min, respectively, which exhibited no significant difference compared with Mock cells (16.3 min; Fig. S3 B). However, the

cells expressing Sgo1 Δ SET (28 min) were delayed in chromosome segregation compared with the cells expressing Sgo1 WT (20 min; Fig. 4, C and D). As SET binding to Sgo1 can inhibit the Sgo1-cohesin interaction that is essential for centromeric cohesion protection, the above results imply that SET and the SET-Sgo1 binding may promote chromosome segregation via disrupting the Sgo1-cohesin interaction. However, we cannot completely rule out the possibility that the delayed chromosome segregation might be caused by other mitotic defects induced by SET depletion or expression of Sgo1 Δ SET, such as subtle kinetochore-microtubule attachment defects.

We further attempted to confirm the importance of the SET-Sgo1 binding in chromosome segregation using the Sgo1-binding mutant SET 3K. As exogenous SET was always expressed at much higher levels than endogenous SET, we were only able to assess the role of SET 3K in chromosome segregation under the condition of its overexpression. Interestingly, chromosome segregation was slightly delayed in RPE-1 cells overexpressing SET WT compared with cells overexpressing the Sgo1 binding-deficient mutant 3K (Fig. S3 C). Moreover, a higher incidence of chromosome segregation defects was also observed in cells overexpressing GFP-SET WT than 3K (Fig. S3 D). Taken together, these results further support that the SET-Sgo1 binding regulates chromosome segregation. Of note, the mechanism of

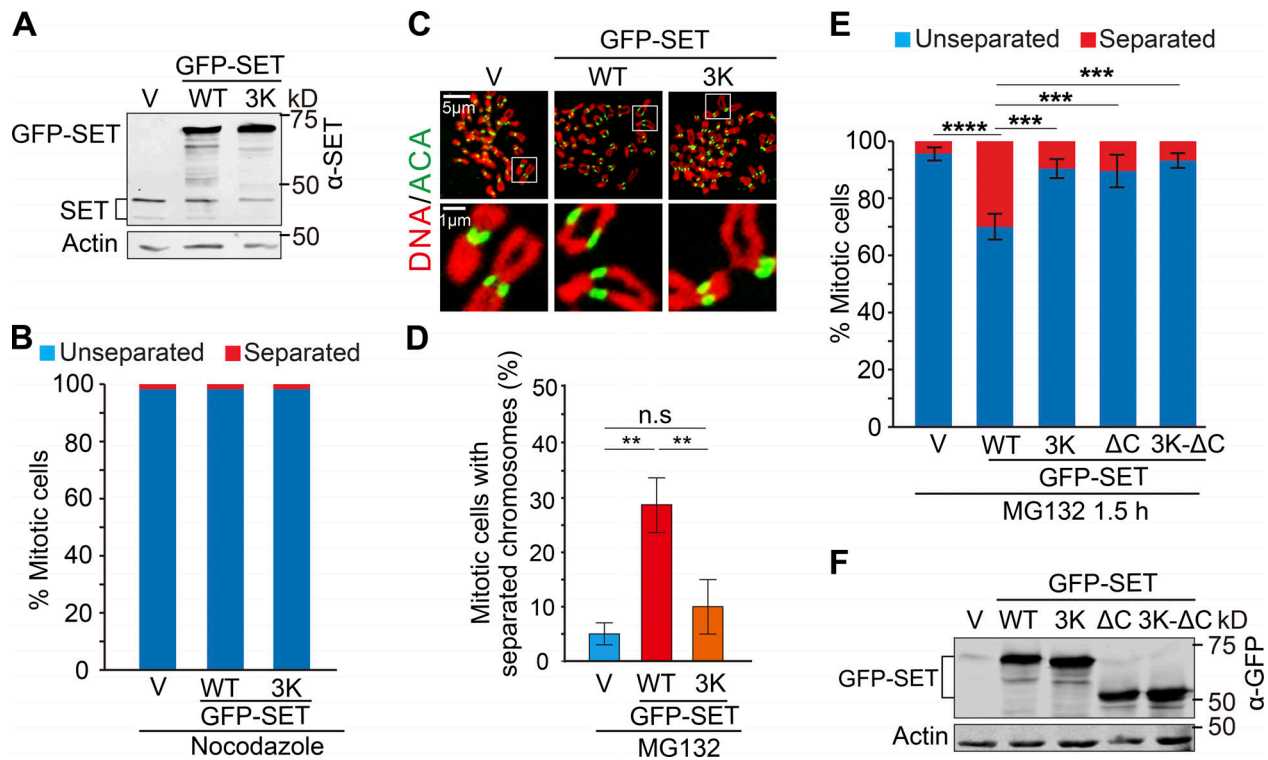


Figure 5. SET overexpression accelerates the occurrence of cohesin fatigue in MG132-arrested cells. (A) Lysates of RPE-1 cells transfected with vector control (V) or plasmids containing GFP-SET WT or 3K were resolved with SDS-PAGE and blotted with the indicated antibodies. (B) SET overexpression barely affects centromeric cohesion in nocodazole-arrested cells. Nocodazole-arrested RPE-1 cells transfected with vector control (V) or plasmids containing GFP-SET WT or 3K were subjected to chromosome spread. Quantification of unseparated (blue bars) and separated (red bars) sister centromeres is shown here. The average from two independent experiments is shown here. (C) Overexpression of SET WT, not 3K, induces significant centromeric cohesion defects in MG132-arrested RPE-1 cells. Shown here are representative images of chromosome spread from MG132 (3 h)-arrested RPE-1 cells transfected with vector control (V) or plasmids containing GFP-SET WT or 3K. The outlined regions showing unseparated (V and 3K) and separated (WT) sister centromeres are amplified and shown in the bottom panel. (D) Quantification of mitotic cells in C with separated centromeres. The average and standard deviation from three independent experiments are shown here. At least 30 cells were examined for each condition. **, $P < 0.01$. One-way ANOVA was performed followed by pairwise comparisons using Tukey's test. n.s., not significant. (E) Overexpression of SET WT induces cohesion fatigue in MG132-arrested HeLa Tet-On cells. MG132 (1.5 h)-treated HeLa Tet-On cells transfected with vectors or plasmids containing GFP-SET WT, 3K, ΔC , or 3K- ΔC were subjected to chromosome spread. Quantification of mitotic cells with separated and unseparated sister chromatids is shown here. The relative intensity was derived from the intensity of Sgo1 signals normalized to one of the ACA signals. At least 60 kinetochores (five per cell) were examined for each condition. The average and standard deviation from at least three independent experiments are shown here. ***, $P < 0.001$; ****, $P < 0.0001$. One-way ANOVA was performed followed by pairwise comparisons using Tukey's test. (F) Cell lysates in E were resolved with SDS-PAGE and blotted with the indicated antibodies.

the delayed anaphase in SET-WT is very likely different from that in Sgo1 Δ SET. The slight delay for SET-WT is likely derived from weakened centromeric cohesion caused by its overexpression (Fig. 5, C-E), but the delay for Sgo1 Δ SET is due to a prolonged metaphase-to-anaphase transition (Fig. 4, C and D).

SET overexpression accelerates the occurrence of cohesion fatigue in MG132-arrested cells, not in nocodazole-arrested cells

We next wondered if SET overexpression could impair centromeric cohesion in cells, as SET overexpression has been shown to impair the Sgo1-cohesin interaction that is critical for centromeric cohesion protection. To test it, we first examined centromeric cohesion in RPE-1 cells overexpressing SET in the presence of nocodazole, a microtubule-depolymerizing drug that compromises kinetochore attachment by microtubules. Western blots showed that the expression levels of GFP-SET WT and 3K proteins were comparable to one another, and both of them

were higher than endogenous SET proteins (~8–10-fold; Fig. 5 A). Distinct from the previous result that SET overexpression in mouse oocytes caused precocious separation of sister chromatids (Qi et al., 2013), SET overexpression in nocodazole-arrested prometaphase RPE-1 cells did not induce any discernible increase in centromeric cohesion defects compared with mock treatment (Fig. 5 B), suggesting that either the amount of overexpressed SET proteins in our experimental condition does not suffice to completely disrupt the Sgo1-cohesin interaction or overexpressed SET proteins are functionally suppressed in nocodazole-arrested cells. As a matter of fact, we have shown that SET-GFP overexpression in nocodazole-arrested cells was able to moderately reduce but not abolish the Sgo1-cohesin interaction (Fig. 3, B, D, and F).

Elongated treatment of MG132, a drug that arrests cells at metaphase with kinetochores attached by microtubules, will induce centromeric cohesion fatigue (Daum et al., 2011). Thus, compared with nocodazole, MG132 could be used to detect

mild cohesion defects by measuring kinetics of cohesion fatigue. We thereby examined cohesion fatigue in MG132-arrested cells overexpressing SET. MG132 treatment for 4 h only induced cohesion fatigue in 5% of mock RPE-1 cells, whereas it did so in 28% of RPE-1 cells overexpressing GFP-SET WT, suggesting that SET overexpression can accelerate the occurrence of cohesion fatigue (Fig. 5, C and D). Interestingly, although GFP-SET 3K overexpression did also induce a slight increase in cells with cohesion fatigue (10% versus 5%), the extent was much milder than WT overexpression. The similar results were also observed in MG132-treated HeLa Tet-On cells expressing GFP-SET WT or 3K (Fig. 5, E and F, and Fig. S4 A). We also examined the capacity of GFP-SET Δ C and 3K- Δ C in inducing cohesion fatigue in MG132-arrested HeLa Tet-On cells and found that these two mutants, like SET 3K, failed to induce cohesion fatigue (Fig. 5 E). However, as truncation of the SET C-terminus decreased its binding not only to PP2A but also to Sgo1 (Fig. 2 E and Fig. S2 C), the above results might not be sufficient to support that SET directly inhibiting PP2A activity is also involved in this process. As the only detected defect of the SET 3K mutant is in Sgo1 binding, the SET overexpression-induced centromeric cohesion defects, we believe, are likely through disruption of the Sgo1-cohesin interaction. SET was recently shown to be able to evict Sgo1 from chromatin in an *in vitro* system (Krishnan et al., 2017). As a result, the phenotype we observed in cells could be induced by premature dissociation of Sgo1 from both kinetochores and inner centromeres in response to SET overexpression. We therefore quantified the total Sgo1 levels at kinetochores and inner centromeres in HeLa Tet-On cells overexpressing GFP-SET. Surprisingly, no discernible decrease in Sgo1 levels was observed at any of the tested mitotic stages; instead, a slight increase was observed in prometaphase/metaphase cells overexpressing SET (Fig. S4, B and C). Thus, the centromeric cohesion defects caused by SET overexpression in our experimental system are unlikely through prematurely removing Sgo1 away from chromatin.

SET depletion delays the occurrence of cohesion fatigue in MG132-arrested cells and reduces Sgo1 relocation from inner centromeres to kinetochores

We have shown that SET overexpression accelerated the occurrence of cohesion fatigue. We next asked if reducing SET protein levels could delay this process. To test it, we compared the kinetics of cohesion fatigue occurrence in between mock and siSET cells. Western blots demonstrated that SET siRNAs efficiently depleted SET proteins (Fig. 6 A). At time point 0 (without MG132 treatment), the majority of chromosomes in mock and siSET cells maintained robust centromeric cohesion (Fig. 6 B). MG132 treatment for 2 h and 4 h triggered the occurrence of cohesion fatigue in 25% and 75% chromosomes in mock cells, respectively, while only 12% and 37% of chromosomes in siSET cells exhibited cohesion fatigue after MG132 treatment for 2 h and 4 h, respectively, suggesting that SET depletion delays the occurrence of cohesion fatigue. The delayed occurrence of cohesion fatigue might also be caused by increased Sgo1 proteins at kinetochores and inner centromeres induced by SET

depletion. We thereby quantified the total Sgo1 signals at kinetochores and inner centromeres in MG132-arrested mock and siSET cells. No significant increase in Sgo1 signals was observed in siSET cells compared with mock cells (Fig. S4 D). We next transfected RNAi-resistant SET to these SET-depleted cells to test if it could restore cohesion fatigue. Consistently, SET depletion significantly suppressed cohesion fatigue induced by MG132 (Fig. 6 C). The suppression was completely reversed by expression of SET WT, but not SET 3K, strengthening the notion that the SET-Sgo1 interaction is likely involved in this process. As we have previously shown that Sgo1 overexpression is able to delay the occurrence of MG132-induced cohesion fatigue (Liu et al., 2013a), we also evaluated the ability of Sgo1 Δ SET in this process. Consistently, overexpression of Myc-Sgo1 WT or Δ SET both rescued MG132-induced cohesion fatigue, but no significant difference between them was observed, although Δ SET seemingly did so better than WT (Fig. S4 E).

The Sgo1-cohesin interaction is required for Sgo1 localization to the inner centromere. If SET functions to inhibit the Sgo1-cohesin interaction, SET depletion would prevent the removal of Sgo1 from inner centromeres; on the contrary, SET overexpression would promote this process. To determine if this could be the case, we sought to measure the kinetics of Sgo1 removal from inner centromeres to kinetochores in MG132-arrested cells. However, MG132 treatment results in cohesion fatigue (Daum et al., 2011), which forces Sgo1 to relocate to kinetochores because of centromeric cohesin loss, creating a caveat that any factor that regulates cohesion fatigue may indirectly affect Sgo1 localization. We believe that to examine Sgo1 localization only in chromosomes with intact centromeric cohesion could minimize this caveat, because in a portion of these chromosomes, Myc-Sccl was still retained at inner centromeres even though Sgo1 had been relocated to kinetochores (Fig. S4 F), suggesting that Sgo1 can separate from centromeric cohesin without centromeric cohesin loss. Such a phenomenon was also reported previously (Lee et al., 2008). We first examined Sgo1 localization on chromosomes with intact centromeric cohesion in MG132-treated HeLa Tet-On cell-depleted SET. In MG132-treated cells, two major types of Sgo1 localization were observed: two peaks of Sgo1 signals that largely colocalize with the ones of ACA (anti-centromere antibody) signals (category I, kinetochore localization), and one major peak of Sgo1 signals that mainly localizes in between two peaks of ACA signals (category II, inner-centromeric localization; Fig. 6 D). In the absence of MG132 treatment (time point 0), Sgo1 predominantly localized at inner centromeres in the majority of the chromosomes of mock and siSET cells (Fig. 6, D and E). No significant difference was found between them. At 2 h after MG132 treatment, Sgo1 exhibited kinetochore localization in ~70% chromosomes of mock cells, whereas it showed kinetochore localization in only ~30% of chromosomes of siSET cells. At 4 h after MG132 treatment, Sgo1 localized at kinetochores in ~80% of chromosomes of mock cells, but it did so in only ~35% of chromosomes of siSET cells. These results indicate that SET depletion reduces Sgo1 relocation from inner centromeres to kinetochores in metaphase-arrested cells. Thus, SET seems to

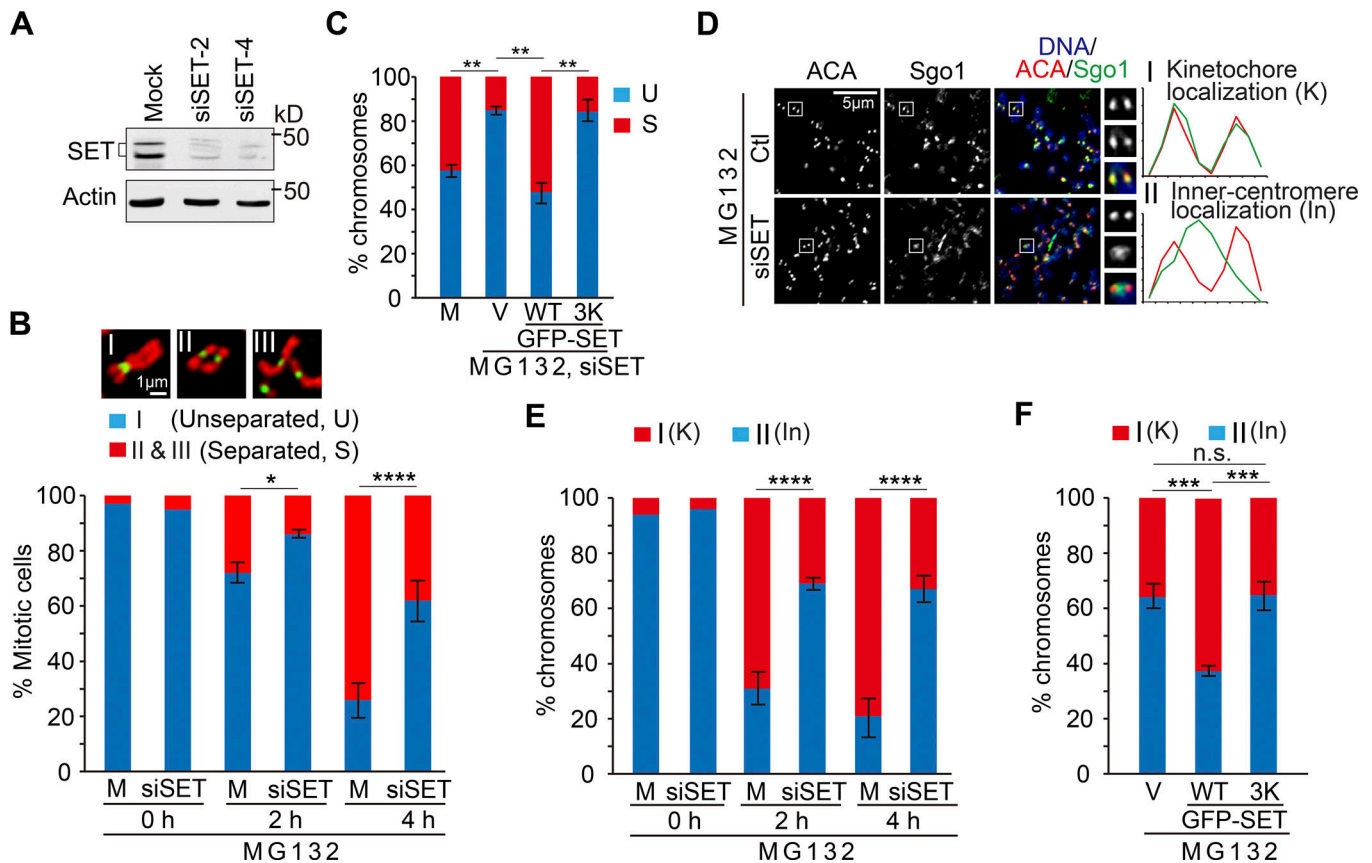


Figure 6. SET depletion delays the occurrence of cohesion fatigue and reduces Sgo1 relocation from inner centromeres to kinetochores in MG132-arrested cells. (A) Lysates of HeLa Tet-On cells with mock treatment or transfected with distinct SET siRNAs (2 and 4) were resolved with SDS-PAGE and blotted with the indicated antibodies. (B) HeLa Tet-On cells with mock or siSET treatment were arrested with MG132 for the indicated time. Three types of chromosome morphology were observed: I, chromosomes with two sister centromeres cohesed; II, chromosomes with two sister centromeres separated but two sister chromatids still paired; and III, chromosomes with sister chromatids scattered. Category I was defined as unseparated chromosomes, and categories II and III were defined as separated chromosomes. Quantification of mitotic cells with unseparated and separated chromosomes is shown. The average and standard deviation from three independent experiments are shown. At least 20 mitotic cells were examined for each condition. *, $P < 0.05$; ****, $P < 0.0001$. One-way ANOVA was performed followed by pairwise comparisons using Tukey's test. (C) HeLa Tet-On cells transiently transfected with vectors or plasmids containing GFP-SET WT or 3K were further treated with SET siRNAs. Cells were treated with MG132 for 2 h before being subjected to chromosome spread. Quantification of unseparated (U) and separated (S) sister chromatids, described in B, is shown here. At least 35 mitotic cells were examined for each condition. The average and standard deviation from two independent experiments are shown here. **, $P < 0.01$. One-way ANOVA was performed followed by pairwise comparisons using Tukey's test. (D) Representative images of MG132 (2 h)-arrested HeLa Tet-On cells with mock treatment or transfected with SET siRNAs. The outlined regions are amplified and shown in the right panel. The plotted curves define the relative localization of ACA (red) and Sgo1 (green) signals. Two types of localization patterns were identified and described in the main text. I, kinetochore localization; II, inner-centromeric localization. (E) Quantification of chromosomes with distinct Sgo1 localization patterns (I and II) in B. Only cells with intact centromeric cohesion were counted. The average and standard deviation from three independent experiments are shown. 50–80 kinetochores (five per cell) were examined for each condition. ****, $P < 0.0001$. One-way ANOVA was performed followed by pairwise comparisons using Tukey's test. (F) Quantification of chromosomes with distinct Sgo1 localization patterns (I and II) in MG132 (1.5 h)-arrested HeLa Tet-On cells transfected with vectors (V) or plasmids containing GFP-SET WT or 3K. Only cells with intact centromeric cohesion were counted. The average and standard deviation from three independent experiments are shown. At least 45 kinetochores (five per cell) were examined for each condition. ***, $P < 0.001$. One-way ANOVA was performed followed by pairwise comparisons using Tukey's test. n.s., not significant.

promote the removal of Sgo1 from inner centromeres to kinetochores in MG132-arrested cells. To further prove this, we then examined Sgo1 localization on chromosomes with intact centromeric cohesion in cells overexpressing SET. As expected, overexpression of SET WT triggered more Sgo1 localization to kinetochores than mock treatment (Fig. 6 F). Interestingly, the Sgo1 binding-deficient mutant SET 3K failed to do so. Taking all the results together, we concluded that SET, by directly binding to Sgo1, may promote the removal of Sgo1 from inner centromeres. We prefer a direct role of SET in the removal of Sgo1 from inner centromeres rather than an

indirect consequence, although we cannot completely rule out the latter.

Localization of SET in nocodazole- and MG132-arrested cells

SET has been shown to localize at centromeres during meiosis (Chambon et al., 2013). We also examined SET localization during mitosis. In nocodazole-arrested HeLa Tet-On cells, two types of SET localization were observed: a bar-like structure (67%) and two foci (33%), both of which localize in between two ACA foci (Fig. S5 A). Interestingly, In MG132-arrested HeLa Tet-On cells, SET largely colocalized with ACA in 93% of

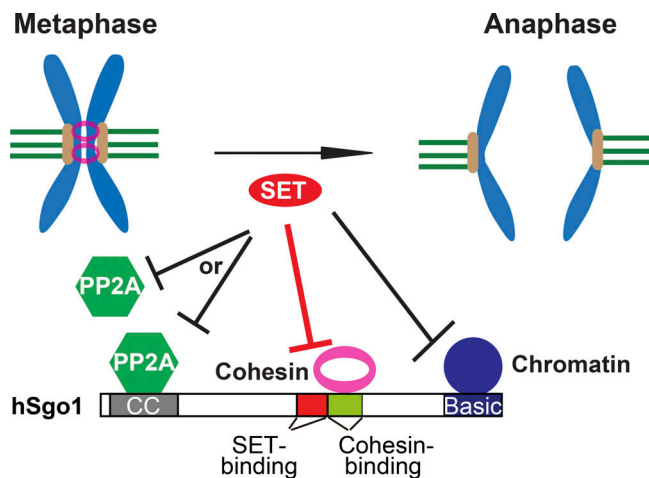


Figure 7. Working model depicting how SET promotes chromosome segregation at the metaphase-to-anaphase transition. At metaphase-to-anaphase transition, by inhibiting the Sgo1-cohesin interaction and/or evicting Sgo1 from chromatin, SET removes Sgo1 from inner centromeres to disable its function of cohesion protection, thereby promoting chromosome segregation. SET may also de-protect centromeric cohesion by directly inhibiting PP2A activity.

kinetochores. Thus, the localization patterns of SET during mitosis are quite similar to the ones of Sgo1 as well as consistent with the findings in a very recent report (Seibert et al., 2019). We then examined the colocalization of SET and Sgo1. We found that SET and Sgo1 largely colocalized to inner centromeres in 59% of the chromosomes in nocodazole-arrested prometaphase cells, and they colocalized to kinetochores in 81% of the chromosomes in MG132-arrested metaphase cells (Fig. S5 B). Notably, we also observed that in ~35% of the chromosomes in nocodazole-arrested cells, SET and Sgo1 partially colocalized with each other. These results suggest that SET and Sgo1 colocalize slightly better in MG132-arrested cells than in nocodazole-arrested cells, but they were insufficient for any solid conclusion. More precise assays are needed for measuring the dynamic regulation of the SET-Sgo1 binding during the cell cycle.

We next examined the localization of SET WT and 3K in nocodazole-arrested HeLa Tet-On cells and found that they both localized to centromeres well (Fig. S5 C), suggesting that SET utilizes separable domains to target to centromeres and regulate cohesion. Interestingly, truncation of the SET C-terminus (227–290) significantly increased its intensity on both centromeres and chromosome arms (Fig. S5 C).

Discussion

At the metaphase-to-anaphase transition, Sgo1 function of cohesion protection must be disabled to allow timely and proper chromosome segregation, but the underlying mechanisms are not fully understood. The Reinberg group has recently shown that SET can evict Sgo1 from chromatin (Krishnan et al., 2017). We here demonstrate that SET is also able to disrupt the Sgo1-cohesin binding. Thus, by inhibiting the Sgo1-cohesin binding and/or evicting Sgo1 from chromatin, SET removes Sgo1 away

from the inner centromere, thereby disabling Sgo1 function of cohesion protection at metaphase-to-anaphase transition (Fig. 7). Therefore, our findings add a novel dimension in understanding how Sgo1 function is disabled.

Although the SET-Sgo1 binding has been identified in various studies, it was not until recently that the biological relevance of this interaction was studied. Results from the Reinberg group and our laboratory both suggest that the SET-Sgo1 binding is critical for timely chromosome segregation. How does this binding promote chromosome segregation? We identified the domain in Sgo1 responsible for SET binding, which is in close proximity to the cohesin-binding domain that is essential for Sgo1 function. The subsequent results showed that SET binding to Sgo1 can inhibit the Sgo1-cohesin interaction in vitro and in cells and may promote timely chromosome segregation at anaphase onset. Thus, we propose that SET is an inhibitor to the Sgo1-cohesin interaction, and this inhibition is important for disabling Sgo1 function. Using an in vitro system, the Reinberg group demonstrated that SET is required for efficiently evicting Sgo1 and Sgo2 from chromatin (Krishnan et al., 2017), suggesting that in addition to inhibiting Sgo1-cohesin interaction, SET binding to Sgo1 is also important for evicting Sgo1 from chromatin. The eviction might be achieved through inhibiting the Sgo1-nucleosome binding as the Sgo1-nucleosome binding is essential for installing Sgo1 on chromatin (Liu et al., 2013a, 2015). Moreover, the Reinberg group and we both found that the SET dimerization domain is critical for SET binding to Sgo1. We further identified several amino acid residues within the dimerization domain that play a critical role in SET-Sgo1 binding. Interestingly, these residues are dispensable for SET dimerization. Thus, SET binds to Sgo1 and dimerizes with itself using distinct sets of residues, even though these residues are in close proximity. In addition to the dimerization domain, we found that the C-terminal domain of SET (residues 227–290) also contributes to the SET-Sgo1 binding, which is congruent with the finding that this region is important for efficiently evicting Sgo1 and Sgo2 from chromatin (Krishnan et al., 2017). Regardless of these detailed mechanisms, all these results define SET as a cellular inhibitor to Sgo1. Notably, although it has been shown that SET can evict Sgo1 from chromatin in an in vitro system (Krishnan et al., 2017), we did not observe any discernible decrease in the Sgo1 levels on chromatin in response to SET overexpression in cells (Fig. S4 C). The underlying reasons are not clear. It is possible that the function of overexpressed SET proteins could be suppressed in our tested conditions.

Sgo1 must keep active at early mitosis to protect centromeric cohesion and inactive at the metaphase-to-anaphase transition to de-protect centromeric cohesion. To coordinate this process, SET, as a Sgo1 inhibitor, and its binding to Sgo1 could also be regulated. Unfortunately, we failed to detect the endogenous SET-Sgo1 binding by immunoprecipitation, which has not been reported either by the Reinberg group, thus preventing us from exploring how the endogenous SET-Sgo1 interaction is regulated at different stages of mitosis. As such, we still examined the regulation of Myc-Sgo1-SET interactions and found no significant difference in between nocodazole-arrested and MG132-arrested cells. Furthermore, we also examined the localization

of SET and Sgo1 and found that they colocalize with each other slightly better in MG132-arrested cells than in nocodazole-arrested cells. However, these results are not conclusive, and more precise assays are needed for measuring the dynamic regulation of the SET–Sgo1 binding during the cell cycle. Alternatively, the SET–Sgo1 interaction might be altered only in a short period of time at anaphase onset. This time window might not be recapitulated by MG132 treatment. Moreover, endogenous Sgo2 was found to bind SET, and this interaction seemed to be regulated by Plk1 activity, suggesting that the endogenous Sgo1–SET binding might also be regulated in a similar manner (Krishnan et al., 2017). However, it should also be noted that SET might differentially regulate Sgo1 and Sgo2 as the major biochemical difference between Sgo1 and Sgo2 is that Sgo1 binds to cohesin during mitosis and Sgo2 does not (Tanno et al., 2010). As a result, Sgo2 is largely dispensable for centromeric cohesion protection during mitosis as well as mitotic progression.

As SET has also been characterized as a cellular PP2A inhibitor (Li et al., 1995, 1996), the phenotype of cohesion fatigue induced by SET overexpression could be a consequence of the direct SET inhibition of PP2A activity. In support of this notion, overexpression of SET ΔC that is defective in binding and inhibiting PP2A failed to induce cohesion fatigue. However, SET ΔC also exhibits decreased binding to Sgo1, making it unclear whether SET directly inhibiting PP2A activity is involved in this process as well. During mitosis, various pools of PP2A have been found at kinetochores, and among them, the pool of Sgo1-bound PP2A has so far been found to be essential for centromeric cohesion protection (Kitajima et al., 2006; Riedel et al., 2006; Tang et al., 2006; Tanno et al., 2010; Suijkerbuijk et al., 2012; Kruse et al., 2013). We have previously shown that the binding of Sgo1 to cohesin protects centromeric cohesion by both bringing Sgo1-bound PP2A in close proximity to cohesin and directly antagonizing Wapl binding to cohesin (Liu et al., 2013b; Hara et al., 2014). Thus, SET binding to Sgo1 could reverse these two processes and peel Sgo1-bound PP2A away from cohesin, thereby annihilating Sgo1-bound PP2A function in cohesion protection. In this sense, the final outcome of disruption of Sgo1–cohesin interactions is still PP2A inhibition, albeit indirectly. Alternatively, SET could remove Sgo1 from inner centromeres through directly inhibiting the activity of other PP2A pools at kinetochores, as PP2A activity per se is also important for maintaining Sgo1 at centromeres (Tang et al., 2006). Regardless, SET may inhibit Sgo1 function by directly removing Sgo1 from inner centromeres and/or directly suppressing PP2A activity. Therefore, we propose that SET de-protects centromeric cohesion by inhibiting Sgo1 and/or PP2A (Fig. 7).

SET overexpression has been found in a variety of types of cancers (Hung and Chen, 2017). Cancer cells often exhibit impaired centromeric cohesion that may represent a major cause of chromosome instability (Barber et al., 2008). In the future, it will be tempting to test whether high levels of SET proteins in cancer cells contribute to the impaired centromeric cohesion. If so, what are the underlying mechanisms? In addition to the well-documented SET–PP2A interaction, SET also interacts with Sgo1 (Krishnan et al., 2017) and p53 (Wang et al., 2016). As SET

overexpression has also been associated with cancer initiation and development (Hung and Chen, 2017), it would be feasible to apply these interactions to understand the underlying mechanisms in the future.

Materials and methods

Mammalian cell culture, lentiviruses, siRNAs, and transfection

HeLa Tet-On cells were cultured in DMEM (Invitrogen) supplemented with 10% FBS and 10 mM L-glutamine. RPE-1 cells were cultured in DMEM: F-12 medium (Invitrogen) supplemented with 10% FBS and 10 mM L-glutamine. Nocodazole and MG132 were purchased from Sigma-Aldrich.

Lentiviral particles were constructed using the pLVX-Puro system (Clontech) in 293T cells. Polyethylenimine–DNA complexes containing pRSV-Rev, pMDLg-pRRE, pMD2.G, and pLVX inserted with genes of interest (Sgo1 WT or ΔSET) were first prepared. Then the assembled complexes were added into cultured 293T cells. After 2 d, cell culture containing virus was collected, filtered, and stored at -80°C for later use.

Plasmid transfection was done using the Effectene reagent (Qiagen) according to the manufacturer's protocols. To generate the inducible stable cell lines, HeLa Tet-On cells were transfected with pTRE2 vectors encoding RNAi-resistant MYC-SGO1 WT or ΔSET (truncated 281–310) and selected with $350\ \mu\text{g ml}^{-1}$ hygromycin (Invitrogen). The surviving clones were screened for expression of the desired proteins in the presence of $1\ \mu\text{g ml}^{-1}$ doxycycline (Invitrogen). To construct the stable cell lines, RPE-1 cells were infected with the lentiviral particles containing MYC-SGO1 WT or ΔSET and selected with $1\ \mu\text{g ml}^{-1}$ puromycin (Sigma-Aldrich).

For RNAi experiments, the siRNA oligonucleotides were purchased from Thermo Fisher Scientific. HeLa Tet-On or RPE-1 cells were transfected using Lipofectamine RNAiMax (Invitrogen) and analyzed at 24–48 h after transfection. The sequences of the siRNAs used in this study are as follows: SET siRNA-2, 5'-GGAUGAAGGUGAAGAAGAU-3' (D-019586-02; Thermo Fisher Scientific); SET siRNA-4, 5'-CGAGUCAACGC AGAAUAA-3' (D-019586-02; Thermo Fisher Scientific); Sgo1 siRNA, 5'-CCUGCUCAGAACCAGGAAA-3'; Sgo2, 5'-TCAAAG ACATTACCTGATA-3'; and Separase siRNA, 5'-GCUUGUGAU GCCAUCCUGATT-3'.

Antibodies, immunoblotting, and immunoprecipitation

The following antibodies were used in this study: anti-centromere antibody (ACA or CREST-ImmunoVision, HCT-0100), anti-Myc (11667203001; Roche), anti-tubulin (62204; Thermo Fisher Scientific), anti-PP2A-A α (Sc-6112; Santa Cruz Biotechnology), anti-histone H3 (A300-823A; Bethyl), anti-histone H3-pS10, anti-Smc1 (A300-055A; Bethyl), anti-Sgo2 (A301-261A; Bethyl), anti-SET (A302-261A; Bethyl; Sc-25664; Santa Cruz Biotechnology) and anti-actin (MA5-11869; Thermo Fisher Scientific). Anti-Sgo1, anti-Sgo1-pT346, anti-GFP, and anti-APC2 antibodies were made in-house as described previously (Liu et al., 2013a; Kim and Yu, 2015).

For immunoblotting, purified or monoclonal antibodies were used at $1\ \mu\text{g ml}^{-1}$ concentration. For immunoprecipitation,

anti-myc or anti-GFP antibodies were coupled to Affi-Prep Protein A beads (Bio-Rad) at a concentration of 1 mg ml⁻¹.

Immunoprecipitation was performed as described previously (Liu et al., 2013b). HeLa Tet-On cells were lysed with lysis buffer (25 mM Tris-HCl, pH 7.5, 50 mM NaCl, 5 mM MgCl₂, 0.1% NP-40, 1 mM DTT, 0.5 μM okadaic acid, 5 mM NaF, and 0.3 mM Na₃VO₄) and 100 U ml⁻¹ Turbo-nuclease (Accelagen). After a 1-h incubation on ice and then a 15-min incubation at room temperature, the lysate was cleared by centrifugation for 20 min at 4°C at 20,817 g. The supernatant was incubated with the antibody beads for 2 h at 4°C. The beads were washed four times with wash buffer (25 mM Tris-HCl, pH 7.5, 100 mM NaCl, 5 mM MgCl₂, 0.1% NP-40, 1 mM DTT, 0.5 μM okadaic acid, 5 mM NaF, and 0.3 mM Na₃VO₄). The proteins bound to the beads were dissolved in SDS sample buffer, separated by SDS-PAGE, and blotted with the appropriate antibodies.

For quantification of Smc1-Sgo1 binding in Fig. 3 B and Myc-Smc1-Sgo1 in Fig. 3 D, masks were generated to cover the Western blotting bands using ImageStudio. After background subtraction, the intensities of Sgo1-immunoprecipitated (Fig. 3 B) or Myc-Sgo1-immunoprecipitated (Fig. 3 D) Smc1 were normalized to the ones of immunoprecipitated Sgo1 (Fig. 3 B) or immunoprecipitated Myc-Sgo1 (Fig. 3 D). Arbitrary units were defined by fold changes of each treated condition (plasmid) relative to control (vector). Arbitrary units were finally analyzed and plotted with Microsoft Excel and GraphPad Prism.

Immunofluorescence and chromosome spread

Chromosome spreads and immunostaining were performed as described before (Liu et al., 2013a). Mitotic cells were swelled in a prewarmed hypotonic solution containing 50 or 75 mM KCl for 15 min at 37°C and then spun onto slides with a Shandon Cytospin centrifuge. Cells were first extracted with ice-cold PBS containing 0.2% Triton X-100 for 2 min and then fixed in 4% ice-cold paraformaldehyde for 4 min. Cells were washed with PBS and then incubated with primary antibodies overnight at 4°C. Cells were washed three times with PBS containing 0.1% Triton X-100 and incubated at room temperature for 1 h with the appropriate secondary antibodies conjugated to fluorophores (Molecular Probes). After incubation, cells were washed again with PBS containing 0.1% Triton X-100, stained with 1 μg ml⁻¹ DAPI, and mounted with Vectashield. The images were taken by a Nikon confocal microscope with a 60× objective. Image processing was performed with ImageJ and Adobe Photoshop. Quantification was performed with ImageJ.

For quantification of total Sgo1 levels at kinetochores and inner centromeres in Fig. S4 C, a mask was generated to mark both the kinetochore and inner centromere on a chromosome. After background subtraction, the intensities of Sgo1 and ACA signals within the mask were obtained in numbers. Relative intensity was derived from the intensity of Sgo1 signals normalized to the one of ACA signals and plotted with the GraphPad Prism software.

Experiments in Fig. 1 H, Fig. 5 B, Fig. 6 C, Fig. S1 D, Fig. S3 D, Fig. S4 D, and Fig. S5 C were repeated at least twice. Experiments in Fig. 5, C and E; Fig. 6, B and D-F; and Fig. S5, A and B, were repeated three times. Sample size is recorded in the figure

legends. No specific statistical methods were used to estimate sample size.

Time-lapse microscopy

RPE-1 cells were transfected with H2B-GFP (Fig. 4) or H2B-mCherry (Fig. S3 C). Long-term imaging was performed, and images were collected every 5 min for 10–12 h at 37°C and 5% CO₂ using a Nikon confocal microscope eclipse Ti2 equipped with an environment chamber that controls temperature and CO₂, 20× objective, and a DIC N2 camera. Image panels displaying the elapsed time between consecutive frames were assembled using the software designed for Nikon confocal microscope. The time taken for each cell to progress from NEB to anaphase onset (chromatid separation) was calculated in minutes and plotted in GraphPad Prism. For the experiments in Fig. 4, ≥45 cells in each condition were counted. Only cells with anaphase initiation were recorded in Fig. 4, C and E, and Fig. S3 A. In Fig. S3 B, cells with anaphase initiation for Mock, WT, or ΔSET were recorded, and cells with final cell death or abnormal mitotic exit for vectors were recorded. In the depicted graphs, each dot represents one cell, and the horizontal and vertical lines indicate the mean and standard deviation, respectively, of the population. The experiments in Fig. 4 were repeated at least two times, and the results were reproducible. Quantification was performed based on the results from a single experiment. Standard deviation was calculated using GraphPad Prism. All the samples analyzed were included in quantification. Sample size was recorded in the figure and its corresponding legends. No specific statistical methods were used to estimate sample size.

Protein purification

His₆-SET (full length) proteins were purified as follows: BL21 *Escherichia coli* cells expressing His₆-SET proteins incubated in lysis buffer (50 mM Tris-HCl, 100 mM NaCl, 5 mM imidazole, 0.1 mM EDTA, and proteinase inhibitors, pH 8.0). After sonication, the lysate was cleared by centrifugation and incubated with Ni beads. The beads were washed with wash buffer (50 mM Tris-HCl, 300 mM NaCl, 15 mM imidazole, and 0.1 mM EDTA, pH 8.0) to remove unbound proteins. To obtain the His₆-SET proteins bound to Ni beads, elution was done with elution buffer (50 mM Tris-HCl, 50 mM NaCl, and 300 mM imidazole, pH 8.0). Finally, eluted proteins were changed to storage buffer (20 mM Tris-HCl, 50 mM NaCl, and 0.1 mM EDTA, pH 7.5) and concentrated.

To obtain GST-SET proteins and GST-Sgo1 fragments, BL 21 *E. coli* cells expressing the proteins were incubated with lysis buffer (10 mM Na₂HPO₄, 1.8 mM KH₂PO₄, 2.7 mM KCl, 137 mM NaCl, 10% glycerol, and protease inhibitors (Roche), pH 7.4) and sonicated. The lysates were cleared by centrifugation, and the supernatants were incubated with glutathione-Sepharose 4B beads to allow binding of GST-tagged proteins. After incubation, beads were washed with wash buffer (10 mM Na₂HPO₄, 1.8 mM KH₂PO₄, 2.7 mM KCl, and 137 mM NaCl, pH 7.4) and then eluted with elution buffer (10 mM Na₂HPO₄, 1.8 mM KH₂PO₄, 2.7 mM KCl, 137 mM NaCl, and 10 mM reduced glutathione, pH 7.4). Eluted proteins were then stored in storage buffer (20 mM Tris-HCl and 50 mM NaCl, pH 7.5) at –80°C for later use.

Recombinant cohesin complexes containing SA2 (residues 80–1,060) and Scc1 (residues 281–420) were generated according to the previous report (Hara et al., 2014). As for cohesin complexes, Hi5 insect cells (Sigma-Aldrich) were coinfecting with baculoviruses containing SA2 (residues 80–1060) and Scc1 (residues 281–420) and harvested at ~50 h after infection. The lysis buffer (50 mM Tris-HCl, pH 7.7, 150 mM KCl, 0.1% [vol/vol] Triton X-100, and a protease inhibitor cocktail) was used to resuspend the cells. After sonication and centrifugation, the supernatant was applied onto Ni²⁺-NTA resin (Qiagen) pre-equilibrated with the lysis buffer and rock-incubated at 4°C overnight. The resin was then washed sequentially with wash buffer I (50 mM Tris-HCl, pH 7.7, 1.2 M KCl, and 10 mM imidazole) and wash buffer II (20 mM Hepes, pH 7.4, 100 mM NaCl, and 20 mM imidazole). The SA2-Scc1 complex was eluted with the elution buffer (20 mM Hepes, pH 7.4, 100 mM NaCl, and 50–200 mM imidazole), and His₆ tags were removed by the TEV (tobacco etch virus) and PreScission proteases. The complex was then applied onto a HiTrap Q HP column (GE Healthcare) pre-equilibrated with the buffer (50 mM Tris-HCl, pH 8.5) using an AKTA chromatography system (GE Healthcare). SA2-Scc1 was eluted with a linear salt gradient from 0 to 600 mM NaCl and further applied onto a HiLoad 16/60 Superdex 200 prep-grade column (GE Healthcare) pre-equilibrated with the purification buffer (20 mM Tris-HCl, pH 7.7, 300 mM NaCl, and 5 mM TCEP [tris(2-carboxyethyl)phosphine]). Purified SA2-Scc1 was concentrated and stored at –80°C for later use.

Bulk histone proteins were prepared as described (Liu et al., 2015). Briefly, recombinant *Xenopus laevis* xH2A, xH2B, xH3, and xH4 or human histones hH2A and hH2B were expressed in bacteria as inclusion bodies and purified individually. Histone octamers were formed in the refolding buffer after mixing the four *Xenopus* histones at equimolar ratio and further purified by gel filtration chromatography. The purified histone octamers were dialyzed into the storage buffer (10 mM Tris-HCl, pH 7.5, and 1 mM DTT) and stored at –80°C for later use.

In vitro pull-down assays

To perform binding assays in Fig. 1, B and D, GST beads prebound with GST or GST-tagged proteins were incubated with the indicated prey proteins at 4°C with end-to-end rotation for ≥1 h. Beads were washed with wash buffer (20 mM Tris-HCl, 50 mM NaCl, and 0.1% NP-40, pH 7.5) to remove unbound protein. Proteins bound to the beads were dissolved in SDS sample buffer, resolved in SDS-PAGE, and blotted with the desired antibodies or stained with Coomassie brilliant blue. All the pull-down experiments were repeated at least two times, and the results were reproducible.

For in vitro competition assays in Fig. 3 A, recombinant cohesin complexes containing SA2 (residues 80–1060) and Scc1 (residues 281–420) were incubated with Cdk1-CyclinB1 in the absence or presence of ATP in kinase buffer (20 mM Tris-HCl, 50 mM NaCl, 2 mM MgCl₂, and 1 mM DTT, pH 7.5). The mixture then was further incubated with GST beads prebound with GST or GST-Sgo1 (residues 241–387) proteins in the presence of increasing amount of His6-SET (full length) in buffer (20 mM Tris-HCl, 50 mM NaCl, and 0.1% NP-40, pH 7.5) at 4°C with end-to-end rotation for 1 h. After washing with wash buffer (20 mM

Tris-HCl, 50 mM NaCl, and 0.1% NP-40, pH 7.5), proteins bound to pelleted beads were dissolved in SDS sample buffer, resolved in SDS-PAGE, and blotted with the desired antibodies or stained with Coomassie brilliant blue. This experiment was repeated twice, and the results were reproducible.

For in vitro binding assays in Fig. 2, B and C, and Fig. S2, A and B, the S35-labeled proteins were produced by incubating the pCS2-Myc-Sgo1 or pCS2-Myc-Sgo2 or PCS2-SET (WT or mutants) plasmids in the TNT Quick Coupled Transcription Translation System (Promega) containing 35S-methionine at 30°C for 90 min. Then, the glutathione-Sepharose beads bound to GST-SET (full length; Fig. 2, B and C) were incubated with 35S-labeled Myc-Sgo1 or Sgo2, or the glutathione-Sepharose beads bound to GST-Sgo1 (241–350; Fig. S2 A) or beads covalently coupled with bulk histones using AminoLink kit (Thermo Fisher Scientific; Fig. S2 B) were incubated with 35S-labeled SET WT or mutants at 4°C overnight. The beads bound with proteins were washed four times with TBS containing 0.05% Tween 20 and separated by SDS-PAGE. The gels were stained with Coomassie blue, dried, and analyzed with a phospho-imager (Fujifilm). Intensities of bound proteins were quantified with ImageJ.

Quantification and statistical analysis

The obtained numeric values from Image J were plotted with GraphPad Prism or Microsoft Excel. Averages and standard deviations were calculated using GraphPad Prism or Microsoft Excel and shown in each figure.

A two-tailed *t* test was performed for the experiments with two samples. As for the experiments with more than two samples, differences were assessed using ANOVA followed by pairwise comparisons using Tukey's test. All the samples analyzed were included in quantification. Sample size was recorded in figures and their corresponding legends. No specific statistical methods were used to estimate sample size. No methods were used to determine whether the data met assumptions of the statistical approach.

Online supplemental material

Fig. S1 shows the regulation of SET-Sgo1 interactions over the cell cycle and the localization of Myc-Sgo1 in HeLa Tet-On cells. Fig. S2 demonstrates how we mapped the residues in SET responsible for binding Sgo1 as well as the interaction between Myc-Sgo1 and SET ΔC. Fig. S3 shows chromosome segregation defects in response to SET overexpression. Fig. S4 summarizes Sgo1 levels on chromosomes in cells overexpressing SET or depleted of SET. It also contains the suppression of cohesion fatigue by Sgo1 overexpression and the separation of Sgo1 from centromeric cohesin in MG132. Fig. S5 shows the localization of SET in nocodazole- and MG132-arrested cells.

Acknowledgments

The lentivirus system was a gift from Dr. Yan Dong at Tulane University Health Sciences Center, New Orleans, LA. We also thank Dr. Hongtao Yu at the University of Texas Southwestern, Dallas, TX, for reagents and Dr. Xiaofeng Zhu at Sichuan University, Chengdu, China for advices on

methodology. Mass spectrometric analyses were performed by the Proteomics Core at Louisiana State University School of Medicine.

This work was supported by Tulane startup funds and National Institutes of Health grants P20GM103629 and R01GM124018, awarded to H. Liu.

The authors declare no competing financial interests.

Author contributions: Conceptualization, H. Liu; methodology, H. Liu; investigation, Q. Qu, Q. Zhang, L. Yang, Y.J. Chen, and H. Liu; writing, original draft, H. Liu; writing, review and editing, Q. Qu, Q. Zhang, L. Yang, and H. Liu; funding acquisition, H. Liu; resources, H. Liu; and supervision, H. Liu.

Submitted: 18 October 2018

Revised: 29 March 2019

Accepted: 15 May 2019

References

- Barber, T.D., K. McManus, K.W. Yuen, M. Reis, G. Parmigiani, D. Shen, I. Barrett, Y. Nouhi, F. Spencer, S. Markowitz, et al. 2008. Chromatid cohesion defects may underlie chromosome instability in human colorectal cancers. *Proc. Natl. Acad. Sci. USA*. 105:3443–3448. <https://doi.org/10.1073/pnas.0712384105>
- Chambon, J.P., S.A. Touati, S. Berneau, D. Cladière, C. Hebras, R. Groeme, A. McDougall, and K. Wassmann. 2013. The PP2A inhibitor I2PP2A is essential for sister chromatid segregation in oocyte meiosis II. *Curr. Biol.* 23:485–490. <https://doi.org/10.1016/j.cub.2013.02.004>
- Daum, J.R., T.A. Potapova, S. Sivakumar, J.J. Daniel, J.N. Flynn, S. Rankin, and G.J. Gorbsky. 2011. Cohesion fatigue induces chromatid separation in cells delayed at metaphase. *Curr. Biol.* 21:1018–1024. <https://doi.org/10.1016/j.cub.2011.05.032>
- Hara, K., G. Zheng, Q. Qu, H. Liu, Z. Ouyang, Z. Chen, D.R. Tomchick, and H. Yu. 2014. Structure of cohesin subcomplex pinpoints direct shugoshin-Wapl antagonism in centromeric cohesion. *Nat. Struct. Mol. Biol.* 21: 864–870. <https://doi.org/10.1038/nsmb.2880>
- Hauf, S., I.C. Waizenegger, and J.M. Peters. 2001. Cohesin cleavage by separase required for anaphase and cytokinesis in human cells. *Science*. 293:1320–1323. <https://doi.org/10.1126/science.1061376>
- Herzog, F., A. Kahraman, D. Boehringer, R. Mak, A. Bracher, T. Walzthoeni, A. Leitner, M. Beck, F.U. Hartl, N. Ban, et al. 2012. Structural probing of a protein phosphatase 2A network by chemical cross-linking and mass spectrometry. *Science*. 337:1348–1352. <https://doi.org/10.1126/science.1221483>
- Hung, M.H., and K.F. Chen. 2017. Reprogramming the oncogenic response: SET protein as a potential therapeutic target in cancer. *Expert Opin. Ther. Targets*. 21:685–694. <https://doi.org/10.1080/14728222.2017.1336226>
- Jonak, K., I. Zagoriy, T. Oz, P. Graf, J. Rojas, V. Mengoli, and W. Zachariae. 2017. APC/C-Cdc20 mediates deprotection of centromeric cohesin at meiosis II in yeast. *Cell Cycle*. 16:1145–1152. <https://doi.org/10.1080/15384101.2017.1320628>
- Karamysheva, Z., L.A. Diaz-Martinez, S.E. Crow, B. Li, and H. Yu. 2009. Multiple anaphase-promoting complex/cyclosome degrons mediate the degradation of human Sgo1. *J. Biol. Chem.* 284:1772–1780. <https://doi.org/10.1074/jbc.M807083200>
- Kawashima, S.A., Y. Yamagishi, T. Honda, K. Ishiguro, and Y. Watanabe. 2010. Phosphorylation of H2A by Bub1 prevents chromosomal instability through localizing shugoshin. *Science*. 327:172–177. <https://doi.org/10.1126/science.1180189>
- Kim, S., and H. Yu. 2015. Multiple assembly mechanisms anchor the KMN spindle checkpoint platform at human mitotic kinetochores. *J. Cell Biol.* 208:181–196. <https://doi.org/10.1083/jcb.201407074>
- Kitajima, T.S., T. Sakuno, K. Ishiguro, S. Iemura, T. Natsume, S.A. Kawashima, and Y. Watanabe. 2006. Shugoshin collaborates with protein phosphatase 2A to protect cohesin. *Nature*. 441:46–52. <https://doi.org/10.1038/nature04663>
- Krishnan, S., A.H. Smits, M. Vermeulen, and D. Reinberg. 2017. Phospho-H1 Decorates the Inter-chromatid Axis and Is Evicted along with Shugoshin by SET during Mitosis. *Mol. Cell*. 67:579–593.
- Kruse, T., G. Zhang, M.S. Larsen, T. Lischetti, W. Streicher, T. Kragh Nielsen, S.P. Bjørn, and J. Nilsson. 2013. Direct binding between BubR1 and B56-PP2A phosphatase complexes regulate mitotic progression. *J. Cell Sci.* 126:1086–1092. <https://doi.org/10.1242/jcs.122481>
- Lee, J., T.S. Kitajima, Y. Tanno, K. Yoshida, T. Morita, T. Miyano, M. Miyake, and Y. Watanabe. 2008. Unified mode of centromeric protection by shugoshin in mammalian oocytes and somatic cells. *Nat. Cell Biol.* 10: 42–52. <https://doi.org/10.1038/ncb1667>
- Li, M., H. Guo, and Z. Damuni. 1995. Purification and characterization of two potent heat-stable protein inhibitors of protein phosphatase 2A from bovine kidney. *Biochemistry*. 34:1988–1996. <https://doi.org/10.1021/bi00006a020>
- Li, M., A. Makinje, and Z. Damuni. 1996. The myeloid leukemia-associated protein SET is a potent inhibitor of protein phosphatase 2A. *J. Biol. Chem.* 271:11059–11062. <https://doi.org/10.1074/jbc.271.19.11059>
- Liu, H., L. Jia, and H. Yu. 2013a. Phospho-H2A and cohesin specify distinct tension-regulated Sgo1 pools at kinetochores and inner centromeres. *Curr. Biol.* 23:1927–1933. <https://doi.org/10.1016/j.cub.2013.07.078>
- Liu, H., S. Rankin, and H. Yu. 2013b. Phosphorylation-enabled binding of SGO1-PP2A to cohesin protects sororin and centromeric cohesion during mitosis. *Nat. Cell Biol.* 15:40–49. <https://doi.org/10.1038/ncb2637>
- Liu, H., Q. Qu, R. Warrington, A. Rice, N. Cheng, and H. Yu. 2015. Mitotic Transcription Installs Sgo1 at Centromeres to Coordinate Chromosome Segregation. *Mol. Cell*. 59:426–436. <https://doi.org/10.1016/j.molcel.2015.06.018>
- Matsumoto, K., K. Nagata, M. Okuwaki, and M. Tsujimoto. 1999. Histone- and chromatin-binding activity of template activating factor-I. *FEBS Lett.* 463:285–288. [https://doi.org/10.1016/S0014-5793\(99\)01632-4](https://doi.org/10.1016/S0014-5793(99)01632-4)
- Muto, S., M. Senda, Y. Akai, L. Sato, T. Suzuki, R. Nagai, T. Senda, and M. Horikoshi. 2007. Relationship between the structure of SET/TAF-Ibeta/INHAT and its histone chaperone activity. *Proc. Natl. Acad. Sci. USA*. 104: 4285–4290. <https://doi.org/10.1073/pnas.0603762104>
- Qi, S.T., Z.B. Wang, Y.C. Ouyang, Q.H. Zhang, M.W. Hu, X. Huang, Z. Ge, L. Guo, Y.P. Wang, Y. Hou, et al. 2013. Overexpression of SETβ, a protein localizing to centromeres, causes precocious separation of chromatids during the first meiosis of mouse oocytes. *J. Cell Sci.* 126:1595–1603. <https://doi.org/10.1242/jcs.116541>
- Riedel, C.G., V.L. Katis, Y. Katou, S. Mori, T. Itoh, W. Helmhart, M. Gálová, M. Petronczki, J. Gregan, B. Cetin, et al. 2006. Protein phosphatase 2A protects centromeric sister chromatid cohesion during meiosis I. *Nature*. 441:53–61. <https://doi.org/10.1038/nature04664>
- Saito, S., M. Miyaji-Yamaguchi, T. Shimoyama, and K. Nagata. 1999. Functional domains of template-activating factor-I as a protein phosphatase 2A inhibitor. *Biochem. Biophys. Res. Commun.* 259:471–475. <https://doi.org/10.1006/bbrc.1999.0790>
- Seibert, M., M. Krüger, N.A. Watson, O. Sen, J.R. Daum, J.A. Slotman, T. Braun, A.B. Houtsmuller, G.J. Gorbsky, R. Jacob, et al. 2019. CDK1-mediated phosphorylation at H2B serine 6 is required for mitotic chromosome segregation. *J. Cell Biol.* 218:1164–1181. <https://doi.org/10.1083/jcb.201806057>
- Suijkerbuijk, S.J., M. Vleugel, A. Teixeira, and G.J. Kops. 2012. Integration of kinase and phosphatase activities by BUBR1 ensures formation of stable kinetochore-microtubule attachments. *Dev. Cell*. 23:745–755. <https://doi.org/10.1016/j.devcel.2012.09.005>
- Tang, Z., H. Shu, W. Qi, N.A. Mahmood, M.C. Mumby, and H. Yu. 2006. PP2A is required for centromeric localization of Sgo1 and proper chromosome segregation. *Dev. Cell*. 10:575–585. <https://doi.org/10.1016/j.devcel.2006.03.010>
- Tanno, Y., T.S. Kitajima, T. Honda, Y. Ando, K. Ishiguro, and Y. Watanabe. 2010. Phosphorylation of mammalian Sgo2 by Aurora B recruits PP2A and MCAK to centromeres. *Genes Dev.* 24:2169–2179. <https://doi.org/10.1101/gad.1945310>
- Waizenegger, I., J.F. Giménez-Abián, D. Wernic, and J.M. Peters. 2002. Regulation of human separase by securin binding and autocleavage. *Curr. Biol.* 12:1368–1378. [https://doi.org/10.1016/S0960-9822\(02\)01073-4](https://doi.org/10.1016/S0960-9822(02)01073-4)
- Wang, D., N. Kon, G. Lasso, L. Jiang, W. Leng, W.G. Zhu, J. Qin, B. Honig, and W. Gu. 2016. Acetylation-regulated interaction between p53 and SET reveals a widespread regulatory mode. *Nature*. 538:118–122. <https://doi.org/10.1038/nature19759>
- Yabe, R., N. Fujiwara, T. Mizuno, T. Usui, T. Ohama, and K. Sato. 2014. Characterization of SET/I2PP2A isoforms in dogs. *J. Vet. Med. Sci.* 76: 1235–1240. <https://doi.org/10.1292/jvms.14-0209>